Latest Jurassic–Early Cretaceous synrift evolution of the Torrelapaja Subbasin (Cameros Basin): implications for Northeast Iberia palaeogeography

Aurell, M. (1); Bádenas, B. (1); Castanera, D. (2); Gasca, J.M. (1); Canudo, J.I. (1); Laita, E. (1); Liesa, C.L. (3)

(1) Grupo Araragosaurus-IUCA, Departamento de Ciencias de la Tierra. Universidad de Zaragoza, 50009 Zaragoza, Spain

(2) Institut Català de Paleontologia Miquel Crusafont, Universitat Autònoma de Barcelona, c/Escola Industrial 23, 08201, Sabadell, Barcelona, Spain

(3) Grupo Geotransfer, IUCA, Departamento de Ciencias de la Tierra. Universidad de Zaragoza, 50009 Zaragoza, Spain

ABSTRACT

The reconstruction of the latest Jurassic–Early Cretaceous evolution of the Torrelapaja Subbasin (Cameros Basin, Spain) resulted in the characterization of three synrift sequences (SS-1, SS-2 and SS-3) bounded by major unconformities. Three major NW-SE normal faults combined with smaller scale faults of variable direction (around NE-SW) controlled the sedimentation. The complex geometry of the Torrelapaja Subbasin indicates a main extension direction of NE-SW, and a secondary NW-SE extension. Sedimentation of the Tithonian–middle Berriasian SS-1 occurred in alluvial fan systems, grading upwards to carbonate palustrine-lacustrine environments. A new vertebrate site with large size sauropod bones has been found in the middle part of SS-1. The lower boundary of the uppermost Hauterivian–lower Barremian SS-2 is locally a palaeokarst, with sedimentary infill including three new fossil sites with remains of ornithopod, sauropod and theropod dinosaurs. Sedimentation of SS-2 encompasses distal alluvial terrigenous facies with local palaeosoils and palustrine-lacustrine limestones grading upwards to middle-distal alluvial facies. After a late Barremian–early Albian stratigraphic gap, sedimentation

resumed in coastal flat environments represented by the mudstones with intercalated skeletal (oyster-rich) sandy limestones with carbonaceous plant remains of the SS-3. A middle-late Albian age assignment of SS-3 based on regional correlation is supported by strontium isotopic data. This unit marks the first Early Cretaceous marine incursion in the area from the northern Atlantic realm. This is a notable change of the previous palaeogeographical reconstructions which established that the first marine encroachment occurred in the early Aptian and was sourced from Tethysian domains.

Key words: *Lower Cretaceous, continental sedimentation, extensional tectonics, dinosaurs, palaeogeography, Northeast Iberia*

1. INTRODUCTION

Extensional tectonics in the Iberian Basin rift system (Northeast Spain) around the Jurassic-Cretaceous transition involved a major palaeogeographic change, from the setting of wide shallow-marine Jurassic carbonate platforms, to continental-coastal sedimentation confined to locally subsident basins, subbasins and troughs. The recorded uppermost Jurassic–Lower Cretaceous synrift deposits consist of successive units separated by unconformities, the number and age of which vary from one sedimentary domain to another (e.g., Salas et al., 2001; Mas et al., 2004; Liesa et al., 2019; Aurell et al., 2019b).

The Torrelapaja Subbasin is a relatively small (8x14 km) uppermost Jurassic–Lower Cretaceous subsident area located in the southeastern edge of the Cameros Basin (Mas et al., 2002), in an area found relatively close to the Maestrazgo Basin (Fig. 1A). The critical location of this subbasin between the two main sedimentary domains of the latest Jurassic–Early Cretaceous Iberian Basin rift system makes its analysis relevant to decipher the sedimentary evolution linked to the active extensional tectonics and to understand the palaeogeography of Northeast Iberia during the latest Jurassic–Early Cretaceous. Initial palaeogeographical reconstructions of Northeast Iberia considered that there was no marine connection

between the northern Cameros and the southern Maestrazgo sedimentary domains during the Early Cretaceous (e.g., Canérot, 1974; García, 1982). However, the presence of coastal marine deposits recorded in the upper part of the synrift succession in the Torrelapaja Subbasin was tentatively related to an early Aptian transgressive event sourced from the southern Tethysian realm (Alonso and Mas, 1988, 1993). Based on this assumption, subsequent early Aptian palaeogeographical reconstructions of Northeast Iberia (e.g., Salas et al., 2001; Mas et al., 2004; Suarez-González et al., 2013) proposed a marine connection between the Cameros and Maestrazgo sedimentary domains through a narrow NW-SE trending seaway located in the central part of the Iberian rift system. However, the data and interpretation reported in our work does not support this Aptian marine connection.

Another point of interest of the uppermost Jurassic–Lower Cretaceous synrift successions of the Iberian Basin rift system is the abundant presence of dinosaur fossil sites. The Cameros Basin has an important record of dinosaur ichnites, especially in the provinces of Soria and La Rioja (e.g., Hernández-Medrano et al., 2005; Moratalla and Hernán, 2010; Pérez-Lorente, 2015). Dinosaur fossil bones are known but in less abundance (e.g., Canudo et al., 2010, Fuentes-Vidarte et al., 2016; Isasmendi et al., 2020). Within the osteological record of Cameros, the Barremian–Aptian in the western domain (Burgos province) stands out by its richness and high number of dinosaur type localities (e.g., Torcida Fernández et al., 2017). Towards the east, the dinosaur fossil record is scarcer. In particular, dinosaur fossil occurrences described so far in the Torrelapaja Subbasin are local and fragmentary (Royo-Torres et al., 2012; Rey-Martínez and Royo-Torres, 2014). However, the data reported here show that this subbasin offers great possibilities of a new significant vertebrate fossil record.

The main aim of this work is to characterize the latest Jurassic–Early Cretaceous tectono-sedimentary evolution of the Torrelapaja Subbasin. Previous work on the area provided relevant structural, stratigraphic and micropaleontological data (Schudack, 1987; Alonso and Mas, 1988, 1990; Martín-Closas, 1989; Guimerà et al., 2004; Sacristán-Horcajada et al., 2011, 2012), but there is a lack of a comprehensive and systematic study of the recorded sedimentary synrift successions. Accordingly, the

objectives of this work are: (1) to reconstruct the structure of the area, with the identification of different sets of normal faults that controlled the tectono-sedimentary evolution; (2) to provide an updated stratigraphic and sedimentological framework of the uppermost Jurassic–Lower Cretaceous synrift successions, in order to reconstruct the depositional setting and its sedimentary evolution; (3) to precise the age and palaeoenvironment of the new dinosaur fossil sites found in the course of our field work, and those previously reported; (4) to discuss on the impact of the obtained results to a better understanding of the palaeogeographic evolution of Northeast Iberia. Data and interpretations provided here can be relevant for future tectono-sedimentary and paleontological research both on the studied subbasin and nearby basins of Northeast Iberia.

2. GEOLOGICAL SETTING

The Torrelapaja Subbasin is defined here to include the Bigornia and Bijuesca troughs identified in previous works (Mas et al., 2002; Guimerà et al., 2004; Sacristán-Horcajada et al., 2011, 2012). This subbasin is located in the southeastern edge of the Cameros Basin (Fig. 1A), a large extensional basin bounded by the so-called North and South Cameros faults. The Cameros Basin records an up to 8 km-thick uppermost Jurassic–Lower Cretaceous dominant continental successions in its depocentral areas (e.g. Mas et al. 2004, 2019; Guimerà et al., 2004; Casas et al., 2009; Clemente, 2010). The Torrelapaja Subbasin is located between the South Cameros Fault and the Carabantes Fault System (Fig. 1B).

The Mesozoic stratigraphy of the study area is summarized in Figure 2. The Variscan basement is unconformably overlain (D1 in Fig. 2) by the Triassic units deposited coeval to the initial stages of the Mesozoic rifting. A regional angular unconformity is also common between the synrift Triassic and postrift Jurassic sequences (San Román and Aurell, 1992; D2 in Fig. 2). The Jurassic sequence consists of marine limestones and marls with variable overall thickness in the areas located north and south to the South Cameros Fault. A nearly 1,000 m-thick marine Jurassic succession is recorded northwards

(Navarro-Vázquez, 1991), whereas south of this fault, the Jurassic is substantially reduced (c. 400 m-thick near Bijuesca village). Marine Jurassic sedimentation ended with the lower Kimmeridgian reefal, oolitic and bioclastic limestones of the Torrecilla Fm (Alonso and Mas, 1990). During the rest of the Kimmeridgian the marine areas were progressively shifted eastwards into the Tethysian domains of the Maestrazgo Basin (e.g., Bádenas and Aurell, 2001; Aurell et al., 2019a), resulting in the mid-Kimmeridgian regional prerift unconformity (D3 in Fig. 2).

The uppermost Jurassic–Lower Cretaceous synrift succession in the Torrelapaja Subbasin studied here consists of up to 500 m-thick siliciclastic and carbonate deposits that have been assigned to the Bijuesca, Ciria, Torrelapaja and Escucha formations (Fig. 2), following the lithostratigraphy used in previous regional studies (Schudack, 1987; Martín-Closas, 1989; Guimerà et al., 2004). The age of the lower units was constrained by ostracod and charophyte biostratigraphy by Martín-Closas (1989) and U. Schudack and M. Schudack (2009), respectively. The Bijuesca and Ciria formations developed within the Tithonian–middle Berriasian, whereas the Torrelaja Fm was assigned to the latest Hauterivian–early Barremian age. An uppermost Albian regional unconformity separates the studied synrift sequences from the postrift Upper Cretaceous successions (D4 in Fig. 2), which include the continental sandstones and mudstones of the uppermost Albian–middle Cenomanian Utrillas Fm (up to 270 m in thickness), followed by the 450–550 m-thick shallow marine Cenomanian–Campanian carbonate units (Alonso et al. 1993; García et al., 2004).

3. MATERIALS AND METHODS

The reconstruction of the sedimentary evolution of the Torrelapaja Subbasin reported here is based on stratigraphical, sedimentological, structural and palaeontological data acquired following extensive field work, geological mapping and logging, complemented with a review of the published information. The workflow relevant to this research consisted of: (1) structural analysis and geological mapping with a

combination of fieldwork and analysis of high-resolution aerial imagery; (2) stratigraphical and sedimentological analysis based on logging of the synrift uppermost Jurassic–Lower Cretaceous successions in selected outcrops (see Fig. 3 for location), suplemented by petrographical analysis of rock hard samples (limestones, sandstones) in thin sections and by mineralogical composition of muddy lithologies; (3) palaeontological fieldwork including the recovery of macrovertebrate remains by surface collection, the microfossil sampling of muddy lithologies in selected fossil-bearing horizons, and location within the geological framework of the new and previously described dinosaur fossil sites; and (4) review and integration of data sets, that resulted in the delineation of updated regional maps showing the palaeogeography of the Northeast Iberia at significant time intervals.

The dinosaur bearing-horizons have been sampled for the analysis of their micropaleontological content (screen-washed samples of 2–5 kg). Moreover, three well-preserved oyster shells found in the upper part of the synrift succession in the Bigornia trough were sampled for strontium-isotopic analysis. The $^{87}Sr/^{86}Sr$ isotopes were determined with a TIMS-Phoenix thermal ionization mass spectrometer at the *CAI Geocronología y Geoquímica Isotópica* of the *Universidad Complutense de Madrid* (Spain). Isotopic data were corrected for possible ^{87}Rb interferences and were normalised to a value of 0.1194 for $^{87}Sr/^{86}Sr$ in order to correct possible mass-fractionation. During the period of analysis, the NBS-987 standard gave an average $^{87}Sr/^{86}Sr$ value of 0.710245 ± 0.000019, which was used to correct the measured values from a possible deviation referred to the standard. The analytical error of the $^{87}Sr/^{86}Sr$ ratio referred to 2σ was 0.01%.

4. STRATIGRAPHIC REMARKS AND STRUCTURE OF THE TORRELAPAJA SUBBASIN

The geological mapping of the area including the Torrelapaja Subbasin (Figs. 3 and 4) shows the distribution of lithostratigraphic units and main structural elements. The subbasin is bounded to the northeast by the southwest-dipping Malanquilla Fault and, to the southwest, by the northeast-dipping Carabantes Fault System (Carabantes Fault; Guimerà et al., 2004). The northeast-dipping Berdejo Fault

(or Cardejón Fault in Guimerà et al., 2004) separates the northern and southern Bigornia and Bijuesca troughs. The uppermost Jurassic (Tithonian)–Lower Cretaceous sedimentary succession of the Torrelapaja Subbasin characterized in this work is arranged in three synrift sequences bounded by major unconformities that can be traced across the study area (Fig. 2): (1) synrift sequence-1 (SS-1) includes the alluvial deposits of the Bijuesca Fm and the lacustrine to palustrine limestones of the Ciria Fm; (2) synrift sequence-2 (SS-2) is formed by the mixed siliciclastic and carbonate continental succession of the Torrelapaja Fm; (3) synrift sequence-3 (SS-3) is characterized by a transitional continental to marine succession, with oyster-rich sandy-limestones with abundant plant debris, followed by coal-bearing sandstones and shales typical of the Escucha Fm. Selected key field views of the synrift units and bounding surfaces in the Bijuesca (Fig. 5) and in the Bigornia troughs (Figs. 6 and 7) are provided.

The lower boundary of SS-1 is the subaerial exposure surface developed on top of the prerift Jurassic marine limestones. This discontinuity has an associated stratigraphic gap encompassing at least the late Kimmeridigian. The individualization of the Torrelapaja Subbasin as a depositional area began with the sedimentation of SS-1. The sequence includes two vertically and laterally related continental units: the alluvial conglomerates, sandstones and mudstones of the Bijuesca Fm, and the palustrine-lacustrine limestones of the Ciria Fm (Fig. 5A). Most of the normal faults that were active during sedimentation of SS-1 are NW-SE trending. Moreover, the northwestern Bigornia trough is compartmentalized by an additional set of normal faults with perpendicular orientation (NE-SW). In the uplifted blocks, SS-1 is very reduced and fossilizes normal faults affecting the marine Jurassic units (Fig. 4A-B; see also Alonso and Mas, 1988, 1990; Sacristán-Horcajada et al., 2012). In the most subsident areas of the northwestern Bigornia and Bijuesca troughs (Fig. 4A-C), the unit form thick successions (up to 350–400 m; see also Alonso and Mas, 1990 and Sacristán-Horcajada et al., 2011, 2012), and the erosive gap of the underlying marine Jurassic rocks is reduced. There, the lower boundary of SS-1 is generally a low-relief paraconformity developed on top of the lower Kimmeridgian Torrecilla Fm (Fig. 5C). In the less subsident areas of the southeastern Bigornia trough, the basal conglomerates of the Bijuesca Fm are 0–30 m-thick

and the sequence is dominated by the limestones of the 20–80 m thick Ciria Fm.

The lower boundary of SS-2 (Torrelapaja Fm) is the major unconformity between the lacustrine limestones of the Ciria Fm (lower-middle Berriasian) and the continental terrigenous of the Torrelapaja Fm (uppermost Hauterivian-lower Barremian). An irregular incised (some dm´s in deep) karstic surface is frequently observed on top of the lacustrine limestones of SS-1 (Figs. 6A and 7A). The karstic cavities are filled by argillaceous mudstones, which may include a rich assemblage of disarticulated vertebrate remains (see section 6). Angular unconformities are commonly observed in the southeastern Bigornia trough, where some of the NE-SW faults that were active during the sedimentation of SS-1 are fossilized by SS-2 (Fig. 8). The Torrelapaja Fm (SS-2) includes a high variety of continental facies, mainly muddy facies (from shales to calcareous mudstones) and intercalated limestones, conglomerates and sandstones (Figs. 6C–F and 7D). The unit reaches maximum thickness of 60–80 m in the southeastern Bigornia trough (Fig. 4B). By contrast, the unit is absent or very reduced in the southern Bijuesca trough and in the northwestern edge of the Bigornia trough, where the postrift sandstones of the Utrillas Fm usually overlay the SS-1 (Fig. 5A).

The lower boundary of SS-3 is a regional angular unconformity, which locally fossilizes normal faults that were active during sedimentation of previous sequences (Fig. 3). SS-3 may directly overlay SS-1, as observed in the northwestern part of the Bigornia through, in the outcrops located south of Ciria (Fig. 4A; see Alonso and Mas, 1988; Guimerà et al, 2004). The Escucha Fm (SS-3) is only found in the Bigornia trough. Maximum thickness of the unit measured northeast of Berdejo village is around 50 m. There, the unit consists of shales and burrowed micaceous sandstones rich in plant remains, with intercalation of sandy skeletal limestones and abundant oyster debris (Fig. 7E-F). Its upper part is poorly exposed or eroded across the Torrelapaja Subbasin and consists of sandstones and shales with interbedded coal (lignite) levels. Lignite levels of the Escucha Fm were quarried south of Ciria village, in Vallehermoso (Fig. 4A). A borehole in this locality revealed the presence of a 33 m-thick succession of shales and siltstones

193 including intercalation of dm- to m-thick lignite beds (IGME, 1984). In its type locality, the Escucha Fm
194 has a similar lithological evolution, with a lower member dominated by sandy skeletal (oyster rich) levels
195 and a middle-upper part with abundant lignite levels (e.g., Querol et al., 1992). The upper boundary of
196 SS-3 is the major angular unconformity, which involved block tilting and erosion previous to the
197 deposition of the postrift deposits. The postrift Utrillas Fm rests on a low-angle unconformity and
198 fossilizes normal faults that were active during the sedimentation of the previous synrift sequences, as
199 observed east of Torrelapaja (Fig. 4B) or south of Bijuesca (Fig. 4C).

200

201 **5. FACIES ANALYSIS: PALEOENVIRONMENTAL RECONSTRUCTION**

202 ***5.1. Synrift sequence 1: Alluvial to palustrine-lacustrine systems***

203 The SS-1 sedimentary system has been characterized in the most complete Bijuesca log (Sacristán-
204 Horcajada et al., 2011), complemented with new data of Las Cañadas log, located in the southeastern
205 Bigornia trough (see LC1 and BJ logs respectively in Figs. 4B and C). Further information of the
206 sedimentary evolution of SS-1 in the northwestern Bigornia trough is provided in Sacristán-Horcajada et
207 al. (2012).

208 The terrigenous clastic succession of the Bijuesca Fm represents deposition from proximal to distal
209 alluvial fans (Fig. 9A). In Bijuesca, the lower part of the succession is dominated by fining-upward
210 sequences of matrix-supported conglomerates with sandstone and limestone clasts. Inverse grading is
211 also observed. These deposits were interpreted as debris flow deposits of proximal alluvial fans
212 (Sacristan-Horcajada et al., 2011). The middle part of the Bijuesca Fm consist of clast-supported
213 conglomerates with cm-sized limestone pebbles and normal grading, fining-upward to cross-bedded
214 sandstones and red mudstones (Fig. 5F, G) deposited in channels and flood plains of middle alluvial fan
215 areas. Red mudstones with local root traces and intercalated cross-bedded sandstones dominate in the

upper part of the unit and represent deposition in a distal alluvial fan. Mudstones and nodular (bioturbated) limestones with characean algae and gastropods at the topmost part of the unit indicates the setting of carbonate palustrine subenvironments. The new dinosaur fossil site of La Atalaya occurs in a palustrine level found at this topmost part, in the transition to the overlaying Ciria Fm (Fig. 5A-B; see section 6).

During SS-1 there was an expansion of the lacustrine system of the Ciria Fm over the alluvial fans of the Bijuesca Fm. The Ciria Fm was interpreted as a low-gradient ramp margin lake, mostly sourced from spring waters (Sacristan-Horcajada et al., 2011). Carbonate saturated waters could be related to discharges from karstic aquifers sourced from the Jurassic marine limestones. The Ciria Fm is characterized by meter-thick sequences from lacustrine to palustrine facies (Fig. 9A-B). Lacustrine facies encompass tabular meter-thick bioclastic limestones with characean algae, ostracods, gastropods and bivalves. Limestones with bioclastic lime mudstones and wackestones represent deposition in low-energy lacustrine areas. Bioclastic wackestones to packstones with intraclasts, quartz grains and black pebbles formed in littoral to shallow lacustrine areas. The palustrine facies corresponds to nodular/brecciated limestones bearing similar skeletal components than the lacustrine limestones, but including evidences of edaphic processes (e.g., nodulization, brecciation, root traces, black pebbles, fenestral porosity; Fig. 9C). The palustrine-lacustrine facies also include gray mudstones and marls and local oncolitic limestones with cm-thick oncoids with bioclastic cores in Las Cañadas log (Fig. 9B-D).

In Las Cañadas the Ciria Fm includes sandstones and clast-supported conglomerates with sharp flat or channelized bases and limestone pebbles. Their intercalation within the palustrine-lacustrine facies reflects deposition in the distal alluvial fan area, with sheet flood deposits or channelized flows entering in the lake.

5.2. Synrift sequence 2: Distal alluvial fans and shallow lakes

Facies analysis of sequence SS-2 (Torrelapaja Fm) is mainly based on the data collected in three logs located in the eastern subsident areas of the Bigornia trough (see LC, VT and VJ logs in Fig. 4B). Three terrigenous muddy facies have been differentiated based on colour and mineralogy (Fig. 10). Ochre to purple mudstones and ochre to violet marlstones/calcareous mudstones include levels rich in Fe-pisoids and root traces/hydromorphic soils and local reworked skeletal debris (ostracods, charophytes and vertebrate remains). They represent deposition in distal alluvial plains with local vegetated areas and lateritic soils. These facies are similar to those found in lateritic palaeosoils in age-equivalent units characterized in the southern Maestrazgo Basin, as in the lower Blesa Fm (Oliete Subbasin: Laita et al., 2020). In contrast, gray marlstones/calcareous mudstones have more abundant ostracods, charophytes and plant debris and some reworked Fe-pisoids, and preferentially accumulated in palustrine to shallow lacustrine areas.

Limestones include a high variety of palustrine to shallow lacustrine facies (Fig. 11A). Bioclastic and fenestral bioclastic limestones (wackestones/packstones, occasional grainstones) with abundant bivalves, gastropods, ostracods and characean algae and some quartz grains (silt to medium sand), dominate. The bioclastic limestones encompass subfacies with accumulated broken bivalves and gastropods (Fig. 11B) or ostracods (Fig. 11C), both produced by hydrodynamic sorting by high-energy events in lacustrine subenvironments. Other group of subfacies is dominated by ostracod and charophytes deposited in quiet lacustrine areas (Fig. 11D). The fenestral bioclastic limestones with abundant microcracks and root traces formed in palustrine areas (Fig. 11E). Two additional grain-supported facies, tufa limestones and intraclastic/litoclastic sandy limestones are also present (Fig. 11A). Tufa limestones include oncolitic subfacies with entire and broken oncoids (up to few cm-size) and intraclasts (bioclastic facies, phytoclasts) in the matrix (Fig. 11F), as well as phytoclastic subfacies with mm- to cm-size clasts of coated plant stems and stromatolites, oncoids and oncoid fragments (Figs. 6F and 11G). The tufa limestones formed in palustrine-lacustrine areas as indicated by their intercalation within gray marlstones/calcareous mudstones (Fig. 11A). The intraclastic/litoclastic facies is a mixture of

poorly sorted and variably rounded grains, including mm- to few cm-size lithoclasts (quartzite and Jurassic limestones), intraclasts (e.g., muddy and bioclastic facies), oncoid fragments and quartz sand grains (Fig. 11A). Nature of grains and lenticular geometries with channelized bases indicate deposition by high-energy floods carrying lithoclasts from emerged areas and eroding both distal plain and palustrine-lacustrine deposits.

Conglomerates and sandstones appear both as isolated tabular or lenticular beds and bed packages (dm to few m-thick). The conglomerates are clast-supported with subangular to subrounded clasts up to 10 cm in size and granule to sand matrix. They have usual channelized bases, planar- and trough cross bedding, cross- and parallel lamination, and normal gradation (Fig. 6E). Conglomerates with quartzite (Paleozoic) and limestone (Jurassic) clasts dominate in the eastern section (Valdelavieja), intercalated within distal alluvial plain facies (Fig. 11A). In contrast, conglomerates including only quartzite clasts are recorded in Valdelatorre log. Fine to medium quartz sandstones have usual planar- and trough cross bedding, cross- and parallel lamination, local ripples (Fig. 6C) and bioturbation (vertical traces). Sandstones occasionally include coarse grains (quartzite and limestone clasts, intraclasts of lacustrine-palustrine facies, Fe-pisoids, oncoid fragments) and bioclasts (bivalves, charophytes, ostracods). The vertical relationships of sandstones and conglomerates with terrigenous muddy facies indicates that they represent channels in middle-distal alluvial plain, reaching also subaqueous palustrine-lacustrine areas. In turn, the isolated packages of conglomerates with quartzite clasts (Fig. 11A) indicate a different source and are interpreted as channels of ephemeral braided streams within the plain.

The described facies have a lateral and vertically preferential distribution, which allow differentiating three sedimentary stages (Figs. 10A and 12). Argillaceous Stage 1 corresponds to the sedimentary infill on the paleokartic surface developed in the boundary between SS-1 and SS-2. It is dominated by muddy facies of argillaceous composition (Fig. 11B) deposited in a distal alluvial plain with vegetated areas and local lateritic soils. Lacustrine-palustrine areas comprise several vertebrate fossil sites (see section 6).

Carbonate-dominated Stage 2 reflects a rise in water level that led to the expansion of lacustrine-palustrine areas and the increase in carbonate content in the distal plain (marlstone/calcareous mudstones: see Fig. 10B), but also a coeval record of alluvial clastic input (sandstones) roughly from the north and south (Figs. 11 and 13). In Stage 3, increase of terrigenous-clastic input resulted in the setting of an asymmetrical sedimentary system. Southwards, middle-distal alluvial fan channels (conglomerates with quartzite and limestone clasts, sandstones and muddy facies of predominant siliceous composition: Fig. 10B) developed, and there was a significant reduction of lacustrine-palustrine areas to ponds. The northern area was dominated by an alluvial-fluvial plain with terrigenous mudstone facies and with ephemeral braided streams (conglomerates with quartzite pebbles).

5.3. Synrift sequence 3: coastal sedimentation

The Escucha Fm has been logged and sampled in an outcrop located south of Valdelavieja, where a relatively thick succession (50 m) has been preserved from the post-rift erosion (Fig. 13A). There, the Escucha Fm is dominated by yellowish to brown mudstones with dm- to m-thick intercalations of sandy bioclastic limestones and sandstones. The terrigenous mudstones are mostly covered, but local small outcrops allow to identify bivalves (including *Trigonia* bivalves and oyster shells of *Exogyras*) and thin (few cm) levels rich in plant debris. The interbedded sandy bioclastic limestones (packstones) have variable proportions of oyster fragments, whole and fragmented gastropods and serpulids, and quartz grains (fine to medium sand). There are also echinoids spines, ostracods, brachiopods, carbonaceous debris and both muddy and sandy intraclasts (Figs. 7F and 13B). The bivalve (oyster) sandy (quartz sand grains) limestones are packstones characterized by accumulated debris of oysters, together with few serpulids, gastropods and carbonaceous debris (Fig. 13C). These two facies have common bioturbation with sedimentary infill consisting of silty lime mudstone texture. The top of the beds can be encrusted and ferruginous, with frequent pholadid borings. Fine-grained sandstone beds with cross bedding and cross- and parallel lamination are locally intercalated within the limestones. They contain lithic peloids in

312 the matrix and few bivalve debris.

313 Deposition of plant-rich terrigenous mudstones took place in low-energy terrestrial-coastal areas with
314 certain vegetal cover. Episodic marine flooding is indicated by the presence of levels with marine
315 bivalves. The sandy bioclastic limestones and sandstones represent deposition in a marine (probably
316 restricted embayed) area colonized mainly by oysters, gastropods and serpulids, and/or due to high-
317 energy events (storms) carrying quartz sand and skeletal debris from the open marine area.
318 Hydrodynamic sorting probably controlled the deposition of carbonate-rich and sandy beds, from well-
319 sorted accumulations of oysters in the bivalve sandy limestones, to poorly sorted sandy bioclastic
320 limestones with muddy and sandy intraclasts, to finer-grained sandstones. Bioturbation recorded in
321 limestones took place after the high-energy events.

322

323 **6. DINOSAUR FOSSIL SITES: DESCRIPTION AND STRATIGRAPHIC SETTING**

324 During the course of this investigation four new fossil dinosaur sites have been found. The *La Atalaya*
325 *site*, located 500 m southwest of Bijuesca village (see LA in Fig. 3), is up to now the only occurrence from
326 SS-1. The other three sites including dinosaur remains have been found in the lowermost levels of SS-2,
327 in the distal alluvial muddy facies (stage 1) that fills the irregular karstic surface developed on top of Ciria
328 Fm (Figs. 10A and 12A). The *Corrales de Valdelavieja site* is located about 2 km to the northeast of
329 Berdejo (see CV in Figs. 4B and 10A). The *Corrales de Las Cañadas site* is found 1.5 km northeast of
330 Torrelapaja village (see CC1 in Fig. 4B). The *Valdelatorre site* is located 1.7 km east from Torrelapaja
331 village (see VT in Fig. 4B and 10A). In this section we provide a brief description of their fossil content.
332 Besides, the data reported here have allowed to precise the stratigraphic setting of some previously-
333 known sites from the Bigornia trough (Royo-Torres et al., 2012; Rey-Martínez and Royo-Torres, 2014).

334 The *La Atalaya fossil site* yields a large-sized limb bone fragment and other large-sized caudal vertebra

assigned to Sauropoda indet. (Fig. 5D-E). Other vertebrate remains recovered by surface collection are an archosaur rib fragment and some crocodylomorph osteoderms. The marly levels found in this fossiliferous interval also hosts a microfossil assemblage including charophytes (poracharaceans), ostracods (cyprideans), gastropods (planorbids and other two taxa), archosaur teeth (mainly crocodylomorphs) and eggshells. This site is included in a bed of palustrine nodular limestone facies found at the uppermost part of the Bijuesca Fm (Figs. 5A-B and 9A). Edaphic process linked to root bioturbation produce nodulization and brecciation of these palustrine facies. However, the nodular limestone of the fossiliferous site is in detail a laterally discontinuous carbonate conglomerate with rounded clasts (Fig. 5D) produced by remobilization, transport and accumulation of the nodules and breccia generated by the edaphic processes. This conglomerate bed laterally passes to marls with root traces. Its location in the topmost part of the Bijuesca Fm points towards its age is around the Tithonian-Berriasian transition. The Bijuesca Fm is assumed to be mostly Tithonian in age, although the precise location of the Tithonian-Berriasian boundary within this unit is uncertain (Martín-Closas, 1989). The early-middle Berriasian age of the overlaying Ciria Fm is locally constrained by charophyte biostratigraphy (Martín-Closas, 1989), particularly by the association of *Atopochara trivolvis var. horrida* and *Nodosoclavator bradleyi* found in the upper part of this unit (see Fig. 4A for location of the sampled point).

The *Corrales de Valdelavieja fossil site* (lowermost Torrelapaja Fm) includes two theropod vertebrae (Fig. 6B) plus other indeterminate remains found in close contact to the karstic surface within the first stage of muddy infill of the palaeokarst (ochre to red marlstones/calcareous mudstones; Fig. 10A). An ornithopod (iguanodontian) tooth was also recovered from the overlaying intraclastic/litoclastic sandy limestone. In addition, an isolated spinosaurid theropod tooth crown, which is slightly lateromedially compressed and ornamented with longitudinal ridges was found *ex-situ* in a boulder of intraclastic/litoclastic facies that forms part of the infill of the paleokarst. Terrigenous muddy facies filling the palaeokarst (see sample CV1 in log VJ2, Fig. 10A) also includes a microfossil assemblage with latest

Hauterivian–early Barremian charophyte remains (*Atopochara trivolvis ancora, A.t. triquetra, Globator maillardii var. trochiliscoides)*, ostracods (cyprideans and other unidentified groups), eggshell fragments, lissamphibian bone fragments and gastropods. Above this interval, samples CV2 and CV3 and has yielded an early Barremian charophyte association with *Atopochara triviolvis* var. *triquetra* (typical form), *Clavator harrisii* var. *harrisii, Clavatoraxis* sp and *Charaxis* (see VJ2 log in Fig. 10A and Fig. 6A for sample location).

In the *Corrales de Las Cañadas fossil site* (lowermost Torrelapaja Fm), a set of isolated macrovertebrate remains was found within the first stage of infill of the paleokarstic surface (ochre to red mudstones: Fig. 10A). The most significant fossil material comprises a sauropod humerus (Fig. 7B), a fragmentary theropod ilium, and a saurischian vertebral centrum. Other indeterminate remains were found *ex situ*, possibly eroded from the karstic infill. A poor microfossil assemblage of latest Hauterivian–early Barremian age has been identified in this level (see sample LC1 in log LC, Fig. 10A). It includes remains of ostracods (mainly cyprideans) and scarce charophytes (utriculi of *Atopochara trivolvis ancora* and *A.t. triquetra*), some of them showing reworking features.

In the *Valdelatorre fossil site* (lowermost Torrelapaja Fm) an ornithopod vertebra was found *ex-situ*, very close to the palaeokarstic surface developed on top of the Ciria Fm. Therefore, it is not possible to ascertain whether it comes from the palaeokarst infill or was eroded from the overlaying muddy/marly levels. The sediment sampling in a gray marlstone/calcareous mudstone bed on top of the vertebrate-bearing bed (see VT1 microfossil sample in log VT, Fig. 10A) allowed to characterize an early Barremian charophyte assemblage dominated by abundant utriculi of *Atopochara trivolvis triquetra* (typical form) along with thalli of *Clavatoraxis* sp. Also frequent are ostracods (several taxa, including cyprideans), eggshell fragments and microvertebrate remains dominated by undetermined lissamphibian bone fragments along with crocodylomorph teeth (bernissartiids and goniopholidids). Moreover, osteichthyan remains are present in less abundance (teeth of Lepisosteiformes and Amiiformes, and ganoid scales).

384 The composition of this microfossil assemblage resembles to those of other lower Barremian successions
385 reported in alluvial to shallow lacustrine settings from the Iberian Basin (e.g., Gasca et al., 2017).

386 In the area of Corrales de Valdelavieja and Valdelatorre, additional vertebrate sites were previously
387 reported by Royo-Torres et al. (2012) and Rey-Martínez and Royo-Torres (2014). These authors found
388 ornithopods and isolated remains of theropod and sauropod dinosaurs from five different sites named
389 BJ-1 to BJ-5 (see Figs. 4B and 10A for location of the most significant BJ1 and BJ5 sites). In particular,
390 Royo-Torres et al. (2012) described cranial and postcranial material of an ornithopod specimen in BJ-1
391 site, and their phylogenetic analysis consider it as a basal styracosternan. This site is found in meter 27 of
392 the VT log, towards the lower part of the Torrelapaja Fm (see Figs. 6D and 10A). Rey-Martínez and Royo-
393 Torres (2014) describe a distal end of a sauropod tibia in BJ-5 site, which is located 1 m above the base of
394 the Torrelapaja Fm (see VJ2 log in Fig. 10A). The authors assumed that all the BJ sites were included in
395 the Ciria Fm, and were "Tithonian and with some doubt Berriasian" in age. However, the review of these
396 fossil sites show that they are actually included in the lower part of the Torrelapaja Fm, and are
397 therefore early Barremian in age.

398

399 **7. AGE OF SYNRIFT SEQUENCES AND REGIONAL CORRELATION**

400 Below we review the age of the three identified synrift sequences based in previous information and
401 new data obtained in this work. According to the age assignment provided, the possible equivalence of
402 the sequences defined in the Torrelapaja Subbasin to the units defined in the depocentral areas of the
403 Cameros Basin and in the western domains of the nearby Maestrazgo Basin is proposed and discussed
404 (Fig. 14).

405 ***7.1. Synrift sequence 1: Tithonian-middle Berriasian***

406 As indicated above, relevant data to precise the age of SS-1 is the presence of an early-middle Berriasian

charophyte association found in the upper part of the Ciria Fm with *Atopochara trivolvis var. horrida* and *Nodosoclavator bradleyi* (Martín-Closas, 1989). Moreover, U. Schudack and M. Schudack (2009) identified a rich Berriasian ostracod association, with different species of *Cypridea, Theriosynoecum, Mantelliana* and *Darwinula* that points to freshwater environments for the sedimentation of the Ciria Fm. Accordingly, at least the upper part of the of SS-1 (Ciria Fm) was coeval to the sedimentation of the lower-middle Berriasian depositional sequence (Oncala Gr) defined in the Cameros Basin (DS-III in Clemente, 2010; DS-3 in Quijada et al., 2013 and Mas et al., 2019).

The facies evolution recorded in the Torrelapaja Subbasin during the sedimentation of SS-1 (from alluvial fan clastics to lacustrine limestones) shows that this unit corresponds to a single depositional sequence. If a sequence-to-sequence correlation is done, SS-1 would be equivalent to the DS-III (Oncala Gr) of the Cameros Basin. However, the particular tectono-sedimentary evolution of the Torrelapaja Subbasin compared to the depocentral areas of the Cameros Basin leaves open the possible equivalence of the lower part of the SS-1 to older Tithonian depositional sequences defined in the Cameros Basin (i.e. Tera Group; DS I–II in Clemente, 2010 or DS 1–2 in Mas et al., 2019). In Figure 14 we suggest the possible equivalence of the lower part of SS-1 with the DS-II (upper Tera Group), as previously proposed in Sacristán-Horcajada et al. (2012).

7.2. Synrift sequence 2: uppermost Hauterivian-lower Barremian

The data reported here give further support to the latest Hauterivian–early Barremian age proposed for the Torrelapaja Fm in previous works. Martín-Closas (1989) found a latest Hauterivian-earliest Barremian association with *Atopochara trivolvis triquetra* (primitive form), *Globator maillardii var. trochiliscoides* and *Clavator calcitrapus* in an isolated outcrop of the Torrelapaja Fm located south to Ciria village (see Fig. 4A for location of the sampled point). U. Schudack and M. Schudack (2009) also report in a rich-assemblage of Hauterivian-early Barremian freshwater ostracods, including different species of *Cypridea, Theriosynoecum, Fabanella, Mantelliana* and *Darwinula* genera. As indicated above (section 6), the

analysis of the lowermost levels of Torrelapaja Fm in Valdelavieja and Las Cañadas logs has yielded a microfossil assemblage with utriculi of *Atopochara trivolvis* var. *ancora* and *A.t.* var. *triquetra* varieties, and *Globator maillardii var. trochiliscoides* (samples LC1 and CV1, Fig. 10). Moreover, the marly levels found in the lower part of the Torrelapaja Fm in the Valdelavieja-Valdelatorre area has yielded an early Barremian charophyte association with abundant *Atopochara trivolvis* var*. triquetra* (typical form) (samples VT1, CV2 and CV3, Fig. 10).

According to Martín-Closas (1989) and Clemente (2010), the Torrelapaja Fm was deposited coeval to the lower part of the Enciso Group (Fig. 14). However, the age of the Enciso Group has been debated (see Martín-Closas, 1989; U. Schudack and M. Schudack, 2009; Clemente, 2010; Suárez-González et al., 2013; Moreno-Azanza et al., 2016; Muñoz et al., 2020). The late Hauterivian-Barremian age range assigned by Clemente (2010) for the Enciso Group is coherent with the presence of *Atopochara trivolvis triquetra* in the Enciso locality (Schudack, 1987), the abundant late Valanginian–Barremian ostracod association found in the unit (U. Schudack and M. Schudack, 2009), and the presence of the Barremian–Albian dasycladalean *Salpingoporella urladanasi* in the Leza Fm, a lateral equivalent of the Enciso Group including levels with marine fossils (Suarez- González et al., 2013). Recently, Muñoz et al. (2020) propose a mid-Hauterivian to mid-Barremian age range for the Enciso Group based in cyclostratigraphy, with the obtained astrochronological scale fitting within the available biostratigraphic data.

7.3. Synrift sequence 3: middle-upper Albian

In the Bigornia trough, the SS-3 consists of shales and sandy skeletal (oyster-rich) limestones, which grades upwards to a terrigenous mudstone dominated succession with interbedded coal levels. Despite the poor exposure of the SS-3 across the studied area, there is no evidence indicating the existence of a significant sedimentary discontinuity (or angular unconformity) within this succession, that have been assigned here to the Escucha Fm. However, previous work in Bigornia trough (Alonso and Mas, 1988, 1993) considered the presence of a sedimentary discontinuity between the lower (oyster-rich) and upper

455 (coal-rich) successions. The authors suggested an early Aptian age for the oyster-rich succession, based
456 in its tentative correlation to the shallow marine units found more than 120 km southwards to the
457 Torrelapaja Subbasin, in the Maestrazgo Basin. This early Aptian age assignment was also assumed in
458 latter works (e.g., Guimerà et al., 2004; Mas et al., 2004; Suarez-González et al., 2013).

459 There are few exposures of Lower Cretaceous marine units exposed close the Torrelapaja Subbasin. The
460 closest shallow marine succession of Grávalos is found 60 km north of Torrelapaja, in the footwall of the
461 North Cameros thrust. In Grávalos, a 50 m-thick mixed siliciclastic-carbonate succession with skeletal-
462 rich beds (oysters, foraminifera, serpulids, rudists, green algae, echinoderms) have yielded an association
463 of Albian benthic foraminifera with *Flabellammina alexanderi* and *Haplophragmium* sp. (Muñoz et al.,
464 1997). According to these authors, this skeletal-rich succession is conformably overlain by the shales and
465 sandstones with coal levels typical of the middle-upper Albian Escucha Fm. As observed in Torrelapaja,
466 the shallow marine succession of Grávalos is also overlain by the postrift unconformity (Utrillas Fm).

467 The SS-3 of the Torrelapaja Subbasin is regarded here as time-equivalent to the Albian succession of
468 Grávalos, and is therefore proposed to be deposited around the middle-late Albian times (Fig. 14). The
469 middle-late Albian age proposed here for the SS-3 in the Torrelapaja Subbasin based on its correlation to
470 the closest marine unit found in an equivalent stratigraphic position is coherent with strontium isotopic
471 data obtained in our work. The isotopic analysis of three oyster shells (*Exogyra*) found in a yellowish
472 terrigenous mudstone interval within the lower part of the SS-3 (see Fig. 4B for location of the sampling
473 site) have yielded $^{87}Sr/^{86}Sr$ isotopes values of 0.707447, 0.707459 and 0.707460, respectively. Due to its
474 deposition in coastal environments, these values obtained from oyster shells may have abnormally high
475 values reflecting a relatively more radiogenic isotopic signal linked to freshwater input (e.g., Bryant et al.,
476 1995). However, the significance of these strontium values is supported by the similar results obtained
477 from the three well-preserved shells analysed, which fit in turn the expected isotopic Cretaceous values.
478 Combining the age of the underlying Torrelapaja Fm (uppermost Hauterivian-lower Barremian) and of

479 the overlaying Utrillas Fm (uppermost Albian-middle Cenomanian: Alonso et al. 1993; García et al.,
480 2004), and the global marine $^{87}Sr/^{86}Sr$ Cretaceous curve (Bralower et al., 1997; Denison et al., 2003;
481 McArthur et al., 2012), the obtained values are constrained in two different time intervals: late
482 Barremian-early Aptian and middle-late Albian respectively (Fig. 13D). However, the late Barremian-early
483 Aptian age for the SS-3 sequence is unlikely considering not only the major angular an erosive
484 unconformity with the underlying uppermost Hauterivian-lower Barremian SS-2 (Torrelapaja Fm), but
485 also the overall palaeogeography of Northeast Iberia during Early Cretaceous times (see discussion in
486 section 9).

487

488 **8. TECTONO-SEDIMENTARY EVOLUTION OF THE TORRELAPAJA SUBBASIN: REGIONAL IMPLICATIONS**

489 As shown in the previous section, the uppermost Jurassic-Lower Cretaceous record of the Torrelapaja
490 Subbasin is very discontinuous, with sedimentation stages during the Tithonian-middle Berriasian
491 (Bijuesca and Ciria formations), the latest Hauterivian-early Barremian (Torrelapaja Fm), and the middle-
492 late Albian (Escucha Fm), respectively. The angular unconformities developed between the synrift
493 sequences and the onlap geometries (see Fig. 8) should be explained in a context in which deformation
494 and block tilting associated to faulting also occurred during the periods without sedimentary record in
495 the basin.

496 The evolution of the successive synrift stages recorded in the Torrelapaja Subbasin was mostly controlled
497 by the activity of the three major NW-SE trending extensional faults described above: the southwest-
498 dipping Malanquilla Fault, the northeast-dipping Berdejo Fault and the northeast-dipping Carabantes
499 Fault System (Figs. 3 and 15). The Bigornia trough is located very close (< 1-2 km) to the South Cameros
500 Fault (section 1-1'; Fig 15). It has an asymmetric graben geometry, tilted towards the Berdejo Fault (i.e.
501 towards the southwest). The Bijuesca trough, however, has a significant halfgraben geometry, which is
502 indicative of the listric geometry of the border Carabantes Fault System. The asymmetry of both

503 structures suggests their link in depth with the basal detachment of the Malache and South Cameros
504 faults, i.e. with the southeast Cameros Basin. Numerous minor normal faults affect the synrift series,
505 usually in a NW-SE direction and, especially in the Bigornia graben, also in other directions. The latter
506 commonly have a NE-SW direction and dips to the northwest (i.e. towards the Cameros Basin) producing
507 traverse halfgrabens, as those located 1-3 km south of the Ciria village, that highly compartmentalized
508 the Bigornia graben (section 2-2'; Fig. 15). The mapping of these three major faults, along with the
509 identification and other minor scale synsedimentary normal faults allow reconstructing the extension of
510 depositional domains and depocentral areas of the Bigornia and Bijuesca troughs during the
511 sedimentation of SS-1, SS-2 and SS-3 (Fig. 16).

512 During the sedimentation of SS-1, the activity of the Carabantes Fault System resulted in the formation
513 of the Bijuesca halfgraben, which record more than 200 m of continental deposits in its southern
514 depocentral areas (Fig. 16A). This halfgraben structure is suggested by the overlap of the Utrillas Fm
515 (postrift unconformity) on increasingly older units (Ciria and Bijuesca formations and even Upper Jurassic
516 rocks) towards the northeast, that is, towards the Berdejo fault (Fig. 3). The conglomerates of the
517 Bijuesca Fm were sourced by the uplifted marine Jurassic rocks. Palaeocurrent data measured in Bijuesca
518 indicates a source area located to the south (Fig. 16A). The analysis of the nature of limestone clasts of
519 the conglomerates in the well exposed outcrop of Bijuesca reveals a predominance of clasts derived
520 from the erosion of the Middle-Upper Jurassic units in the lower part of the Bijuesca Fm, whereas Lower
521 Jurassic clasts dominate in the conglomeratic beds of the upper part of the unit. This trend can be
522 related to the progressive denudation of the marine Jurassic rocks exposed in the southern uplifted
523 areas (i.e. inverted vertical clast distribution or *normal unroofing sequence;* Colombo, 1994). It is
524 interesting to note that the areas that remained uplifted in the southern margin of the Bijuesca trough
525 during the sedimentation of SS-1 show a very large erosive incision on the marine Jurassic rocks, and the
526 postrift Utrillas Fm overlays the lowermost Jurassic units (see the outcrops south of Bijuesca in Fig. 3).

The combined activity of the Berdejo and Malanquilla faults resulted in the formation of the NW-SE trending Bigornia graben. The composition of the clast found in the conglomerates of the Bijuesca Fm in this graben also indicates a dominant source from the surrounding uplifted marine Jurassic rocks. Palaeocurrent data points to dominance of a southern drainage area at the onset of the sedimentation of SS-1, followed by a northern source during the sedimentation of the middle and upper part of the Bijuesca Fm (Fig. 16A; see Sacristán-Horcajada et al. 2012). Compared to the Bijuesca halfgraben, thickness distribution in Bigornia graben is very irregular due to the activity of a set of NE-SW trending faults (Figs. 15 and 16A). Moreover, the graben was asymmetric, with maximum thickness (c. 350–400 m) measured in the hanging wall of the Malanquilla Fault, but with a thicker sequence expected to occur in the hanging wall of the Berdejo Fault according to structural reconstruction (section 1-1'; Fig. 15). The posrift Utrillas Fm and younger units cover the unit in this area and it prevents the corroboration of this assumption. A 180 m-thick succession was measured in the Berdejo fault zone, but it is located in its southwesternmost fault block, which only recorded a small amount of the displacement of the Berdejo Fault. Such outcrop of the Bijuesca and Ciria formations close to the fault, together with other very close located in the footwall of the fault, clearly point that the sedimentation likely encompassed the entire Torrelapaja Subbasin during this stage, and that the Berdejo and minor intrabasinal faults were only responsible for the changes in thickness of the unit.

The lacustrine-palustrine carbonates of the Ciria Fm shows a large expansion across the entire Torrelapaja Subbasin (Fig. 9). Discrete terrigenous-clastic of sandstones and clast-supported conglomerates intercalated within the palustrine-lacustrine limestones of the Ciria Fm in less subsident areas of the southeastern Bijuesca through (see log CC1 in Fig. 9B) are interpreted as distal alluvial fan deposits sourced by the uplifted areas by the Malanquilla Fault.

During the sedimentation of SS-2 (Torrelapaja Fm), a set of normal faults with variable orientation was active in the Torrelapaja Subbasin (Fig. 16B). The Malanquilla and Berdejo faults were reactivated and

controlled the evolution of the Bigornia trough. The angular unconformity between SS-1 and SS-2 in the southeastern Bigornia trough shows evidence of previous faults that were not active during SS-2 (Fig. 8). According to cartographic data, the set of NE-SW faults that compartmentalized the northwestern Bigornia trough during the previous SS-1 were not reactivated (Fig. 3). However, the activity of these faults should not be ruled out, because a set of faults with variable orientation (E-W to N-S) controlled the sedimentation in the southeastern Bigornia trough (Fig. 16B). The reactivation of the NE-SW faults located to the southeast (near the locality of Malanquilla) probably caused the displacement of the local depocentres associated with intrabasinal halfgrabens towards that direction along the Bigornia trough (see section 2-2': Fig. 15). In the southern Bijuesca through, the local sedimentation and preservation of SS-2 has been related to some minor normal faults (see also Fig. 4C).

After the initial stage of irregular sedimentation at the onset of SS-2 (stage 1), there were two stages with variations in depositional subenvironments, which can be partly linked to the tectonic activity (Fig. 12). Stage 2 records carbonate-dominated distal alluvial muddy flats (marlstones/calcareous mudstones) with local lateritic soils and carbonate shallow lakes in central areas, and very local terrigenous input in the northern and southern marginal areas. In contrast, Stage 3 encompasses a more terrigenous-clastic and asymmetric system, characterized to the south by a middle-distal alluvial fan with sandstone and conglomerate channels bearing both limestone (Jurassic) and quartzite (Paleozoic) clasts, and to the central and norther parts by ephemeral braided streams of quartzite conglomerates and muddy flats (siliceous mudstone). The increase of terrigenous-clastic supply form stage 2 to stage 3 can be related to an increase of tectonic activity, with conglomerates sourced by nearby uplifted Mesozoic-Paleozoic rocks (from the south-southeast) and the braided streams sourced from uplifted Paleozoic rocks located eastwards to the Torrelapaja Subbasin (Fig. 16B).

The sedimentation of SS-3 (Escucha Fm) spreads over the northeastern marginal areas of the Bigornia trough, with thickness around 50 m in the areas located close to the Malanquilla and Berdejo faults (Fig.

16C). The poor exposure of the unit does not allow to reach precisions on the synsedimentary fault activity as in previous sequences. However, the existence of relatively thick accumulation of the coal-bearing successions of the Escucha Fm south of Ciria (Vallehermoso locality: IGME, 1984) suggests the reactivation of a new fault plane related to the Malanquilla Fault and located in the footwall of the former one. There is no evidence of sedimentation of the SS-3 sequence in the Bijuesca trough where the postrift Utrillas Fm unconformably overlay SS-1 or older marine Jurassic units (Fig. 3).

In the northwestern Bijuesca trough, SS-3 unconformably overlay with high angle (>30) the beds of the Bijuesca and Ciria formations, as well as the NE-SW faults and halfgraben structures described for SS-1 south of Ciria (Figs. 3 and 15). Such geometrical disposition suggests the following evolutionary stages (see section 1-1'; Fig. 15): (i) the overall tilting of the SS-1 and SS-2 and of the prerift sequence towards the SW, (ii) an erosional stage that levels the structure, and (iii) the onset of the sedimentation of SS-3, the latter being favoured by the activation of the new fault plane associated to the Malanquilla Fault. At this stage, it is probably that the Bigornia trough could change in graben polarity, with the eastern Malanquilla fault being in turn the master fault of the graben. Similar changes in polarity of faults have been also described in the Maestrazgo Basin (Querol et al., 1992; Capote et al., 2002). The long period of time between the deposition of SS-2 and SS-3 proposed in this work (Fig. 14) is coherent with such a change in polarity in the Torrelapaja Subbasin.

To summarize, the three periods of sedimentation recorded in the Torrelapaja subbasin correlate well with the periods of higher tectonic activity defined by subsidence analysis and regional data in the Cameros and Maestrazgo basins for the Late Jurassic-Early Cretaceous rifting stage (Mas et al., 1993, Salas et al., 2001; Liesa et al., 2006, 2019). This means that the record in this sub-basin is mainly produced and preserved by the differential subsidence associated with the faults. Note how in many cases the three synrift sequences are truncated and bounded by angular unconformities, and in turn are truncated by the postrift unconformity. In fact, in many of the fault footwall blocks, the postrift Utrillas

599 Fm rests almost directly on the Jurassic prerift series (Figs. 3 and 15). This is coherent to the position of
600 this subbasin in a marginal area of sedimentation in relation to the depocentral area of the Cameros
601 Basin.

602 On the other hand, the complex geometry of the Torrelapaja Subbasin, mainly defined by two nearly
603 perpendicular fault sets acting simultaneously, greatly resembles what happens during the Late Jurassic-
604 Early Cretaceous rifting stage in the Cameros Basin and in the marginal subbasins of the Maestrazgo
605 Basin (Platt, 1990; Cortés et al., 1999; Liesa et al., 2006, 2018; Antolín-Tomás et al., 2007; Meléndez et
606 al., 2009; Aurell et al., 2016, 2018). Contemporary multi-directional normal fault activity points to a
607 regime of radial extension. The greater significance of faults in NW-SE direction with respect to those in a
608 NE-SW direction, which defines the main structuring of the Torrelapaja Subbasin in sedimentary troughs
609 (Bigornia and Bijuesca), with respect to those in a NE-SW direction suggests a direction of main NE-SW
610 extension and a secondary NW-SE extension, as it has also been proposed for the Cameros Basin from
611 the analysis of faults, calcite veins and magnetic susceptibility anisotropy (Guiraud and Séguret, 1984;
612 Marqués et al., 1996; García-Lasanta et al., 2014).

613

614 **9. DISCUSSION: THE PALAEOGEOGRAPHY OF NORTHEAST IBERIA REVISITED**

615 The data and review reported here have implications on the reconstruction of the overall
616 palaeogeography of the uppermost Jurassic–Lower Cretaceous Iberian Basin rift system, providing
617 arguments to precise previous reconstructions of Northeast Iberia.

618 The palaeogeographic maps of Figure 17 show the reconstruction around the early Berriasian, the early
619 Barremian and the middle Albian, thus for the three synrift sequences recorded in the Torrelapaja
620 Subbasin, respectively. The studied subbasin is located in the southeastern edge of the Cameros Basin,
621 relatively close to the northwestern Maestrazgo Basin (Fig. 1A). Figure 14 shows the equivalence

between the three synrift sequences recorded in the Torrelapaja Subbasin to those defined in the marginal subbasins of the Maestrazgo Basin. It is noted that the stratigraphic gap associated to the unconformity between the SS-1 and SS-2 in the Torrelapaja Subbasin fits a period of irregular and discontinuous sedimentation both in the Cameros Basin (DS IV-V of Clemente, 2010), and in the Maestrazgo Basin, which shows a gap of variable amplitude associated to the unconformity between the major synrift sequences 1 (Tithonian–Berriasian) and 2 (Valanginian–lower Albian) defined in Liesa et al. (2019).

9.1. Early Berriasian palaeogeography

In the Torrelapaja Subbasin, sedimentation around the Tithonian-Berriasian transition occurred in alluvial fan systems, which grade upwards to the setting of carbonate palustrine-lacustrine environments across the entire sedimentation areas during the Berriasian.

The depocentral areas of the Cameros basin during the Tithonian-middle Berriasian record the different siliciclastic-carbonate formations of the up to 3,800 m-thick Tera and Oncala groups (Gómez-Fernández and Meléndez, 1994). Around the Tithonian-Berriasian transition, the westernmost areas were dominated by braided fluvial systems, that gradually evolved to meandering fluvial systems in the western-central areas (Clemente, 2010). Northwards, these fluvial deposits graded progressively to broad, low-gradient tidal flats traversed by shallow meandering channels. The laterally related carbonate-evaporitic deposits found in the northeastern part of the basin of the lower-middle Berriasian Oncala Group were deposited in saline mudflats, with large sulphate input derived from the episodic incursion of marine waters (Quijada et al., 2013, 2020). Similar sulphur isotopic compositions recorded in the carbonate-gypsum deposits of the Oncala Group and in the Basque-Cantabrian Basin support the connection of the Cameros Basin with marine and transitional areas of the Basque-Cantabrian Basin during Berriasian times (Quijada et al., 2013). The existence of marine incursions is further supported by the presence of scarce miliolids in the eastern Cameros basin in the units deposited around the

646 Tithonian-Berriasian transition: in the Matute Fm (upper Tera Group, DS-II; Fig. 14) and in the upper
647 Oncala Group (Gómez-Fernández and Meléndez, 1994).

648 In the southeastern margin of the Cameros Basin, including the Torrelapaja Subbasin, the abundance of
649 the charophytes *Porochara* and *Mesochara* found in the Ciria Fm suggests the possible episodic setting of
650 brackish waters (Martín-Closas, 1989). The presence of brackish waters around this marginal area could
651 be related to ephemeral marine influence sourced from the north (Basque-Cantabrian Basin). The overall
652 palaeogeography of the Iberian Basin rift system during the Berriasian (Fig. 17A) with the marine
653 sedimentation areas confined to the eastern Maestrazgo Basin (e.g., Aurell et al., 2016, 2019b; Bádenas
654 et al., 2004, 2018; Liesa et al., 2019), makes unlikely an alternative marine source from the Tethysian
655 realm. Also of interest are the lacustrine-palustrine carbonates found eastwards to the Torrelapaja
656 Subbasin, in Ricla (Fig. 17A), which also include abundant *Porochara* and *Mesochara* (Martín-Closas,
657 1989). As proposed by Salomon (1982) these carbonates are regarded here as time counterparts of the
658 Berriasian Ciria Fm. However, this is a tentative correlation, because the recorded charophyte
659 association of Ricla does not provide conclusive information about its age (Martín-Closas, 1989; Soria et
660 al., 1995).

661 ***9.2. Early Barremian palaeogeography***

662 During the early Barremian, most of the Cameros basin was the site of continental sedimentation (Fig.
663 17B). The fluvial systems that dominated the sedimentation in the south-central part of the basin
664 changed towards the northwest to small carbonate lakes, and towards the northeast to a siliciclastic and
665 carbonate-dominated continental setting (Clemente, 2010). Assuming an early Barremian age for the
666 Leza Fm (see discussion above), evidences of marine influence coeval to the sedimentation of the SS-2
667 would be recorded in the northeastern edge of the Cameros Basin, with the relatively abundant
668 presence of dasycladaleans, echinoderms and miliolids in some carbonate levels. The Leza Fm was
669 deposited in a system of coastal wetlands with both freshwater and seawater influence, laterally related

to the fluvio-lacustrine deposits towards the south (Suarez-González et al., 2013). Further evidence of marine influence around the earliest Barremian is indicated by the presence of debris of echinoderms in the siliciclastic-dominated succession of the Enciso Group logged close to Navalsaz village (Muñoz et al., 2020; see Fig. 17B for location).

The discussion about the provenance of the episodic marine incursions to explain the presence of marine skeletal-rich levels in the Enciso Group in the northeastern Cameros Basin can be further approached with the available regional data. Lower Barremian deposits found in the Aguilón Subbasin (north to the Maestrazgo Basin, Fig. 17B) correspond to the ostracod-rich lacustrine deposits of the Aguilón Fm (Fig. 14). In this unit, with the exception of a few *Fabanella boloniensis* (allowing more saline brackish water environments), all identified species of ostracods indicates freshwater environments (U. Schudack and M. Schudack, 2009). Further south, in the Oliete Subbasin, the presence of oyster-rich limestones in the middle part of the Blesa Fm indicates the episodic marine connection with the open-marine areas of the Maestrazgo Basin during the early Barremian (Fig. 17B; Aurell et al., 2018). However, there is no data supporting that these marine incursions could reach the sedimentary domains located further north, in the Aguilón Subbasin or in the eastern Cameros Basin. Similarly, the Artoles Fm in the Galve Subbasin represented sedimentation in coastal to shallow marine environments, whereas towards the northwest, in the Las Parras Subbasin, palustrine-lacustrine marls and limestones, containing fresh-water ostracods and charophytes developed (Camarillas Fm: Fig. 14; Liesa et al., 2019). Moreover, considering that the Barremian–Aptian marine facies are confined to the eastern areas of the Maestrazgo Basin (e.g., García, 1982; Liesa et al., 2019), the connection between the Tethys and the Cameros Basin during this time span is unlikely, and the presence of the marine levels found in the northeastern Cameros Basin (Enciso Group) can be satisfactory explained as exclusively related to northern marine incursions (Fig. 17B).

9.3. Middle Albian palaeogeography

The middle-late Albian successions of the Escucha Fm recorded in the Bigornia trough indicates the

episodic setting of coastal marine sedimentary domains (with oysters, echinoderms and serpulids) in the southeastern marginal areas of the Cameros Basin. The coeval successions of Grávalos, located in the footwall of the North Cameros thrust (Fig. 17C), include more open marine intervals, with abundant rudists. According to Muñoz et al. (1997), there is a gradual transition between these shallow marine facies and the coal-rich transitional successions typical of the Escucha Fm.

Following Clemente (2010), the equivalent unit to the Escucha Fm in the western Cameros Basin is the upper part of the Salas Group, a largely progradational fluvial system with evidence of aeolian facies, unconformably overlain by the postrift sandstones of the Utrillas Fm. Terrigenous input of this fluvial system was sourced from the western uplifted Iberian Massif, and drained the basin towards the north-northeast, passing gradually to a tide-influenced coastal plain. According to Clemente (2010), the middle-upper part of the Salas Group in the Soria-Abejar area includes relatively thick intervals of facies with inclined heterolithic strata and coal of possibly tidal origin. Marine incursions in the eastern Cameros Basin were sourced from the north (Muñoz *et al.*, 1997; Clemente, 2010). An alternative source from the southeastern Tethysian domain is unlikely, since the coastal marine sedimentation during the Albian in the Maestrazgo Basin was confined south to the Oliete Subbasin, in its eastern depocentral areas (Fig. 17C; Querol et al., 1992; García et al., 2004; Liesa et al., 2019).

10. CONCLUSIONS

The review of the stratigraphy, sedimentology, structural evolution and vertebrate fossil record of the synrift deposits of the Torrelapaja Subbasin (southeastern Cameros Basin) presented in this study has provided the following main findings:

1- The evolution of the uppermost Jurassic-Lower Cretaceous Torrelapaja Subbasin was mostly controlled by the activity of the three major NW-SE trending extensional faults: Malanquilla Fault

(southwest-dipping), Berdejo Fault (northeast-dipping) and Carabantes Fault System (northeast-dipping). The subbasin was longitudinally subdivided into the Bigornia and Bijuesca troughs by the Berdejo Fault. The Bigornia trough is located very close to the South Cameros Fault and it recorded the most complete and thicker synrift sedimentary succession.

2- Discontinuous activity of the major NW-SE trending faults combined to other minor faults with variable orientation (around NE-SW trending) resulted in an irregular uppermost Jurassic-Lower Cretaceous sedimentary record. The complex geometry of the Torrelapaja Subbasin reconstructed in this work is defined by this two nearly perpendicular fault sets acting simultaneously. The greater significance of faults in NW-SE suggests a direction of main NE-SW extension and a secondary NW-SE extension, as has also been previously proposed for the Cameros Basin.

3- The sedimentary record of the Torrelapaja Subbasin consist of three synrift sequences (SS-1, SS-2 and SS-3) bounded by major unconformities. These unconformities are related to the reactivation of different sets of faults during the different stages of evolution of the subbasin. The Tithonian–middle Berriasian SS-1 (Bijuesca and Ciria formations) occurs across the entire Torrelapaja Subbasin, whereas the uppermost Hauterivian–lower Barremian SS-2 (Torrelapaja Fm) and the middle–upper Albian SS-3 (Escucha Fm) are recorded with significant thickness only in the northern part of the subbasin, in the Bigornia trough.

4- The large sedimentary record of SS-1 occurs in the Bijuesca trough (up to 220 m) and in the northwestern Bigornia trough, where the presence of NE-SW trending faults involved the presence of highly subsident blocks, with up to 350–400 m-thick deposits. Sedimentation of SS-1 occurred in alluvial fan systems, sourced from the uplifted basin margins, exposing the marine Jurassic carbonate rocks. The progressive degradation of the relief favoured the expansion of the carbonate palustrine to lacustrine environments across the entire sedimentation areas during the early-middle Berriasian. The new discovered vertebrate fossil site of La Atalaya (Bijuesca trough) includes large sized sauropods and

741 crocodylomorphs preserved in palustrine facies, and was most probably formed around the Tithonian-
742 Berriasian transition.

743 5- The boundary between SS-1 and SS-2 is a widespread unconformity associated to an upper Berriasian-
744 lower Hauterivian stratigraphyc gap. The thickest record of SS-2 (Torrelapaja Fm) found in the
745 southeastern part of the Bigornia trough (up to 80 m) was mostly controlled by the activity of the
746 Malanquilla and Berdejo NW-SE trending faults, combined to a set of small-scale faults with variable
747 orientations around NW-SE. A locally deep-incised palaeokarst developed on top of the Berriasian
748 lacustrine carbonates was filled by a few dm-thick multiphase levels of muddy distal alluvial facies
749 around the Hauterivian-Barremian transition. These facies include the new discovered vertebrate fossil
750 sites of Corrales de las Cañadas, Corrales de Valdelavieja and Valdelatorre, with a dinosaur-dominated
751 macrovertebrate record of sauropod, theropod and ornithopod remains. After this stage of condensed
752 and irregular sedimentation, a second early Barremian stage of muddy distal alluvial plains with
753 paleosoils and Fe-pisoids as well as palustrine-shallow lacustrine carbonate systems developed. At the
754 third stage, increased tectonic activity involved larger terrigenous-clastic input sourced from the
755 southeast, and the development of middle-distal alluvial systems, and distal mud flats with small
756 carbonate ponds in the central part of the Bigornia trough.

757 6- The SS-3 (Escucha Fm) includes shales and intercalated sandy-skeletal limestones with abundant
758 oysters and plant debris. This unit is assigned here to the middle-upper Albian based in regional
759 correlation and strontium isotopic data. The widespread presence of oysters and other marine skeletal
760 debris (serpulids, echinoderms) indicates the first marine incursion in the studied basin, with marine
761 waters sourced from the north (Bay of Biscay domain). The overall palaeogeography of the Iberian Basin
762 rift system during the Early Cretaceous reviewed and updated here makes unlikely an alternative marine
763 source from the southeast (Tethysian realm) as suggested in previous works. Accordingly, the results
764 presented here might have further implications for the understanding of the overall evolution of the

latest Jurassic-Early Cretaceous Iberian rifting, as clarifying the distribution in time and space of Thetysian and northern affinities of the different paleogeographical domains, and the causes and processes laying behind.

Acknowledgments

This study was subsidized by the Spanish Ministerio de Economía y Competitividad-ERDF (Project CGL2017-85038-P), the Spanish State Research Agency (Project PID2019-108705GB-I00), as well as by the Aragón Regional Government and the European Regional Development Fund (research groups E18_20R *Aragosaurus: recursos geológicos y paleoambientes* and E32_20R *Geotransfer: investigación geológica para la ciencia y la sociedad*). We thank Prof. Carles Martín-Closas for the assistance in the charophyte determination. We also acknowledge the suggestions provided by the two reviewers (professors Marian Fregenal-Martínez and Bruno Granier) that helped to improve the quality of the original manuscript. We also appreciate the technical assistance of the *Servicio General de Apoyo a la Investigación-SAI*, Universidad de Zaragoza. DC is supported by the *Beatriu de Pinós* postdoctoral programme (BP2017-00195) of the Government of Catalonia's Secretariat for Universities and Research of the Ministry of Economy and Knowledge.

REFERENCES

Allix, P., Burnham, A., Fowler, T., Herron, M., Kleinberg, R., Symington, B. (2011): Coaxing oil from Shale. *Oilfield Review* 22 (4), 4–15.

Alonso, A., Mas, J. R. (1988): La transgresión Aptiense al sur del Moncayo (límite de las provincias de Soria y Zaragoza). *II Congreso geológico de España Vol 1,* Granada: p. 11–15.

787 Alonso, A., Mas, J.R. (1990): El Jurásico Superior marino en el sector Demanda- Cameros (La Rioja-Soria).
788 *Cuadernos de Geología Ibérica*, 14, 173–198.

789 Alonso, A., Mas, J. R. (1993): Control tectónico e influencia del eustatismo en la sedimentación del
790 Cretácico inferior de la cuenca de Los Cameros. *Cuadernos de Geología Ibérica* 17, 285–310.

791 Alonso, A., Floquet, M., Mas, R., Meléndez, A. (1993): Late Cretaceous Platforms: Origin and evolution,
792 Iberian Range, Spain. In: J. A. Toni Simo, R. W. Scott, J. P. Masse (eds*.), Cretaceous Carbonate*
793 *Platforms,* AAPG Memoir 56: 297–313.

794 Antolín-Tomás, B., Liesa, C.L., Casas, A.M., Gil-Peña, I. (2007). Geometry of fracturing linked to extension
795 and basin formation in the Maestrazgo basin (Eastern Iberian Chain, Spain). Revista de la Sociedad
796 Geológica de España, 20, 351-365.

797 Aurell, M., Bádenas, B., Gasca, J.M., Canudo, J.I., Liesa, C., Soria, A.R., Moreno-Azanza, M., Najes, L.
798 (2016): Stratigraphy and evolution of the Galve sub-basin (Spain) in the middle Tithonian-early
799 Barremian: implications for the setting and age of some dinosaur fossil sites. *Cretaceous Research* 65,
800 138–162.

801 Aurell, M., Soria, A.R., Bádenas, B., Liesa, C.L., Canudo, J.I., Gasca, J.M., Moreno-Azanza, M., Medrano-
802 Aguado, E., Meléndez, A. (2018): Barremian synrift sedimentation in the Oliete sub-basin (Iberian
803 Basin, Spain): palaeogeographical evolution and distribution of vertebrate remains. *Journal of Iberian*
804 *Geology*, 44, 285–308.

805 Aurell, M., Bádenas, B., Canudo, J.I., Castanera, D., García-Penas, A., Gasca, J.M., Martín-Closas, C.,
806 Moliner, L., Moreno-Azanza, M., Rosales, I., Santas, L., Sequero, C., Val, J. (2019a): Kimmeridgian–
807 Berriasian stratigraphy and sedimentary evolution of the central Iberian Rift System (NE Spain).
808 *Cretaceous Research* 102, 1–19.

809 Aurell, M., Fregenal-Martínez, M., Bádenas, B., Muñoz-García, M.B., Élez, J., Meléndez, N., de
810 Santisteban, C. (2019b): Middle Jurassic–Early Cretaceous tectono-sedimentary evolution of the
811 southwestern Iberian Basin (central Spain): Major palaeogeographical changes in the geotectonic
812 framework of the Western Tethys. *Earth Science Reviews* 199, 102983.

813 Bádenas, B., Aurell, M. (2001): Kimmeridgian palaeogeography and basin evolution of northeastern
814 Iberia. *Palaeogeography, Palaeoclimatology, Palaeoecology* 168, 291–310.

815 Bádenas, B., Salas, R. and Aurell, M. (2004): Three orders of regional sea-level changes control facies and
816 stacking patterns of shallow carbonates in the Maestrat Basin (Tithonian–Berriasian, NE Spain).
817 *International Journal of Earth Sciences*, 93, 144–162.

818 Bádenas, B., Aurell, M., Gasca, J.M. (2018): Facies model of a mixed clastic-carbonate, wave-dominated
819 open-coast tidal flat (Tithonian-Berriasian, north-east Spain). *Sedimentology* 65, 1631–1666.

820 Bralower, T. J., Fullagar, P. D., Paull, C. K., Dwyer, G. S., & Leckie, R. M. (1997). Mid-Cretaceous strontium-
821 isotope stratigraphy of deep-sea sections. *Geological Society of America Bulletin, 109,* 1421–1442.

822 Bryant, J. D., Jones, D. S., & Mueller, P. A. (1995). Influence of fresh-water flux on $^{87}Sr/^{86}Sr$
823 chronostratigraphy in marginal marine environments and dating of vertebrate and invertebrate
824 faunas. *Journal of Paleontology, 69,* 1–6.

825 Canérot J (1974): Recherches géologiques aux confins des Chaînes ibériques et catalane (Espagne). Ph.D.
826 Thesis. Sc. Nat. Toulouse, ENADISMA, Trabajos de tesis.

827 Canudo J.I., Barco J.L., Castanera D., Torcida-Baldor F. (2010): New record of an enigmatic sauropod in
828 the Jurassic-Cretaceous transition of the Iberian Peninsula (Spain). *Paläontologische Zeitschrift* 84,
829 427–435.

830 Capote, R., Muñoz, J.A., Simón, J.L., Liesa, L.C., Arlegui, L.E. (2002) Alpine tectonics I: the alpine system

831 north of the Betic Cordillera. In: The Geology of Spain (Eds. by W. Gibbons & T. Moreno), The
832 Geological Society, London. pp. 367-400.

833 Casas, A.M., Villalaín, J.J., Soto, R., Gil-Imaz, A., del Río, P., Fernández, G. (2009): Multidisciplinary
834 approach to an extensional syncline model for the Mesozoic Cameros Basin (N Spain). *Tectonophysics*
835 470, 3–20.

836 Clemente, P. (2010): Review of the Upper Jurassic-Lower Cretaceous Stratigraphy in Western Cameros
837 basin, Northern Spain. *Revista de la Sociedad Geológica de España* 23 (3-4), 101–143.

838 Colombo, F. (1994): Normal and reverse unroofing sequences in syntectonic conglomerates as evidence
839 of progressive basinward deformation. *Geology* 22 (3): 235–238

840 Cortés, A.L., Liesa, C.L., Soria, A.R., Meléndez, A. (1999). Role of extensional structures on the location of
841 folds and thrusts during tectonic inversion (Northern Iberian Chain, Spain). Geodinamica Acta, 12(2),
842 113–132.

843 Denison, R.E. Miller, N.R. Scott, R.W., Reaser D.F. (2003): Strontium isotope stratigraphy of the
844 Comanchean Series in north Texas and southern Oklahoma. *Geological Society of America Bulletin*
845 115, 669–682

846 Fuentes-Vidarte, C., Meijide-Calvo, M., Meijide-Fuentes, F., Meijide-Fuentes, M. (2016): Un nuevo
847 dinosaurio estiracosterno (Ornithopoda: Ankylopollexia) del Cretácico Inferior de España. *Spanish*
848 *Journal of Palaeontology*, 31 (2), 407–446.

849 García A. (coord.) (1982): Recapitulación: In: *El Cretácico de España*. Univ. Complutense Madrid, 655–
850 680.

851 García, A. Mas, R., Segura, M., Carenas, B., García-Hidalgo, J. F., Gil, J., Alonso, A., Aurell, M., Bádenas, B.,
852 Benito, M. I., Meléndez, A., Salas, R. (2004): Segunda fase de postrift: Cretacico Superior. In: J. A.

853 Vera, *Geología de España*. Sociedad Geológica de España-Instituto Geológico y Minero, Madrid: 510–
854 522.

855 García-Lasanta, C., Oliva-Urcia, B., Román-Berdiel, T., Casas, A.M., Hirt, A.M. (2014). Understanding the
856 Mesozoic kinematic evolution in the Cameros basin (Iberian Range, NE, Spain). Journal of Strcutural
857 Geology, 66: 84-101.

858 García-Mondéjar, J. (1990): The Aptian-Albian carbonate episode of the Basque-Cantabrian Basin
859 (northen Spain): general characteristics, controls and evolution. In: *Carbonate Platforms: Facies,*
860 *Sequences and Evolution* (M.E. Tucker, J.L. Wilson, P.D. Crevello, J.F. Sargy J.F. Read, Eds.), Blackwell,
861 Int. Assoc. Sedimentologists Special Publication 9, 257–290

862 Gasca, J. M., Moreno-Azanza, M., Bádenas, B., Díaz-Martínez, I., Castanera, D., Canudo, J. I., & Aurell, M.
863 (2017): Integrated overview of the vertebrate fossil record of the Ladruñán anticline (Spain): evidence
864 of a Barremian alluvial-lacustrine system in NE Iberia frequented by dinosaurs. *Palaeogeography,*
865 *Palaeoclimatology, Palaeoecology,* 472, 192–202.

866 Gómez-Fernández, J.C. and Meléndez, N. (1994): Estratigrafía de la Cuenca de los Cameros (Cordillera
867 Ibérica Noroccidental, N de España) durante el tránsito Jurásico-Cretácico. *Revista de la Sociedad*
868 *Geológica de España*, 7, 121–39.

869 Guimerà, J., Mas, R., Alonso, A. (2004): Intraplate deformation in the NW Iberian Chain: Mesozoic
870 extension and Tertiaty contractional inversion. *Journal of the Geological Society, London*. (161), 291–
871 303.

872 Guiraud, M., Séguret, M. (1984). Releasing solitary overstep model for the Late Jurassic-Early Cretaceous
873 (Wealdian) Soria strike-slip basin (North Spain). In: Strike slip deformation, basin formation and
874 sedimentation (K.T. Biddle and N. Crhistie-Blick, eds.). SEPM Spec. Publ. 37, 159-175.

875 Hernández-Medrano, N., Pascual Arribas, C. P., Latorre Macarrón, P., Sanz Pérez, E. (2005). Contribución

876 de los yacimientos de icnitas sorianos al registro general de Cameros. *Zubía*, (23), 79–120.

877 IGME (1984): Exploración de lignitos en las áreas de Casarejos (Soria), Contreras (Burgos), Reznos (Soria),
878 Embid de Ariza-Almazul (Soria-Zaragoza) y Bijuesca-Torrelapaja (Soria-Zaragoza). Instituto Geológico y
879 Minero de España, Ministerio de Industria y Energía, Madrid, 1–120.

880 Isasmendi, E., Sáez-Benito, P., Torices, A., Navarro-Lorbés, P., Pereda-Suberbiola, X. (2020). New insights
881 about theropod palaeobiodiversity in the Iberian Peninsula and Europe: Spinosaurid teeth
882 (Theropoda, Megalosauroidea) from the Lower Cretaceous of La Rioja (Spain). *Cretaceous Research*,
883 116, 104600.

884 Laita, E., Bauluz, B, Aurell, M., Bádenas, B., Canudo, J.I., Yuste, A. (2020). A change from warm/humid to
885 cold/dry climate conditions recorded in lower Barremian clay-dominated continental successions
886 from the SE Iberian Chain (NE Spain). *Sedimentary Geology* 403 (2020) 105673

887 Liesa, C.L., Casas, A.M., Simón, J.L. (2018). La tectónica de inversión en una región intraplaca: La
888 Cordillera Ibérica. Revista de la Sociedad Geológica de España, 31: 23-50.

889 Liesa, C.L., Soria, A.R., Casas, A., Aurell, M., Meléndez, N., Bádenas, B., Fregenal-Martínez, M., Navarrete,
890 R., Peropadre, C., Rodríguez-López, J.P. (2019): The South Iberian, Central-Iberian and Maestrazgo
891 basins. In: Quesada, C., Oliveira, J.T. (Eds.), *The Geology of Iberia: A Geodynamic Approach* Vol. 5.
892 Springer Nature Switzerland AG, Alpine Cycle, pp. 214–228.

893 Liesa, C.L., Soria, A.R., Meléndez, N., Meléndez, A. (2006). Extensional fault control on the sedimentation
894 patterns in a continental rift basin: El Castellar Formation, Galve subbasin, Spain. Journal of the
895 Geological Society of London, 163, 487–498.

896 Marqués, L., Maestro, A., Gil, A., Casas, A..M. (1996). Aportaciones del análisis microestructural a la
897 evolución tectónica del extremo oriental de la Cuenca de Cameros. Geogaceta 20(4), 767-769.

898 Martín-Closas, C. (1989): Els caròfits del Cretaci Inferior de les conques periferiques del Bloc de l'Ebre.
899 PhD thesis. University of Barcelona.

900 Mas, R., Alonso, A., Guimerà, J. (1993). Evolución tectonosedimentaria de una cuenca extensional
901 intraplaca: La cuenca finijurásica-eocretácica de Los Cameros (La Rioja-Soria). Revista de la Sociedad
902 Geológica de España, 6: 129-144.

903 Mas, R., Benito, M. I., Arribas, J., Serrano, A., Guimerà, J., Alonso, A., Alonso-Azcárate, J. (2002): La
904 Cuenca de Cameros: desde la extensión finijurásica-eocretácica a la inversión terciaria – implicaciones
905 en la exploración de hidrocarburos. *Zubía Monográfico* 14, 9–64.

906 Mas, R., García, A., Salas, R., Meléndez, A., Alonso, A., Aurell, M., Bádenas, B., Benito, M. I., Carenas, B.,
907 García-Hidalgo, J. F., Gil, J., Segura, M. (2004): Segunda Fase de rifting: Jurásico Superior-Cretácico
908 Inferior. In: J. A. Vera, *Geología de España*. Sociedad Geológica de España-Instituto Geológico y
909 Minero, Madrid: 503–510.

910 Mas, R., Benito, M.I., Arribas, J., Omodeo-Salé, S., Suarez-Gonzalez, P., Quijada, I.E., Guimerà, J.,
911 González-Acebrón, L., Arribas, M.E. (2019): The Cameros Basin. In: Quesada, C., Oliveira, J.T. (Eds.),
912 *The Geology of Iberia: A Geodynamic Approach* Vol. 5. Springer Nature Switzerland AG, Alpine Cycle,
913 pp. 190–205.

914 McArthur, J.M., Howarth, R.J., Shields, G.A. (2012). Strontium isotope stratigraphy. In F. M. Gradstein, J.
915 G. Ogg, M. D. Schmitz, & G. M. Ogg (Eds.), *The Geological Time Scale 2012* (pp. 127–144). Oxford:
916 Elsevier B.V.

917 Meléndez, N., Liesa, C.L., Soria, A.R., Meléndez, A. (2009). Lacustrine evolution during early rifting: El
918 Castellar Formation (Galve sub-basin, Central Iberian Chain). Sedimentary Geology 222, 64-77.

919 Moratalla, J.J., Hernán, J. (2010): Probable palaeogeographic influences of the Lower Cretaceous Iberian

rifting phase in the Eastern Cameros Basin (Spain) on dinosaur trackway orientations. *Palaeogeography, Palaeoclimatology, Palaeoecology* 295, 116–130

Moreno-Azanza, M., Gasca, J.M., Díaz-Martínez, I., Bauluz Lázaro, B., Canudo Sanagustín, J.I., Fernández, A., Pérez- Lorente, F. (2016): A multi-ootaxic assemblage from the Lower Cretaceous of the Cameros Basin (La Rioja; Northern Spain). *Spanish Journal of Palaeontology*, 31 (2), 305–320.

Muñoz, A., Soria, A., Canudo, J. I., Casas, A. M., Gil, A., Mata, M. P. (1997): Caracterización estratigráfica y sedimentológica del Albiense marino del borde Norte de la Sierra de Cameros. Implicaciones Paleogeográficas. *Cuadernos de Geología Ibérica* 22, 139–163

Muñoz, A., Angulo, A., Liesa, C.L., Luzón, M.A., Mayayo, M.J., Pérez, A., Soria, A.R., Val, V., Yuste, A. (2020). Periodicidad climática y datación astrocronológica del Grupo Enciso en la Cuenca oriental de Cameros (N de España). Boletín Geológico y Minero, 131, 2, doi. 10.21701/bolgeomin.131.2.003.

Navarro-Vázquez, D. (coord) (1991): Mapa Geológico de España, 1:50000. Num 380 (Borobia). Instituto Tecnológico Geominero de España, Madrid.

Pérez-Lorente, F. (2015). *Dinosaur footprints and trackways of La Rioja.* Indiana University Press.

Platt, N.H. (1990). Basin evolution and fault reactivation in the Western Cameros Basin, Northern Spain. Journal of the Geological Society of London 147, 165-175.

Pujalte, V., Robles, S., García-Ramos, J.C., Hernández, J.M. (2004): El Malm-Barremiense no marino de la Cordillera Cantábrica. In: J. A. Vera, *Geología de España*. Sociedad Geológica de España-Instituto Geológico y Minero, Madrid: 288–291.

Querol, X., Salas, R., Pardo, G., Ardevol, L. (1992): Albian coal-bearing deposits of the Iberian Range in northeastern Spain. In: McCabe, J.P., Panish, J.T. (Eds.), Controls and distribution and quality of Cretaceous coals. *Geological Society of America, Special Paper* 267, 193–208.

Quijada, I.E., Suarez-Gonzalez, P., Benito, M.I., Mas, J.R. (2013): New insights on the stratigraphy and sedimentology of the Oncala Group (eastern Cameros Basin): implications for the paleogeographic reconstruction of NE Iberia at Berriasian times. *Journal of Iberian Geology* 39, 313–334.

Quijada, I.E., Benito, M.I., Suarez-Gonzalez, P., Rodriguez-Martínez, M., Campos-Soto, S. (2020): Challenges to carbonate-evaporite peritidal facies models and cycles: Insights from Lower Cretaceous stromatolite-bearing deposits (Oncala Group, N Spain). *Sedimentary Geology,* 408 105752

Rey-Martínez, G, Royo-Torres, R. (2014): Estudio paleontológico de una tibia de dinosaurio saurópodo de la Formación Ciria (Titoniense–Berriasiense) hallada en Berdejo (Zaragoza). *XII Encuentro de Jóvenes Investigadores en Palentología (Boltaña, 2014).* 105–108.

Royo-Torres, R., Gascó, F., Cobos, A. (2012): Dinosaurs from Zaragoza province (Iberian Range, Spain). *Fundamental*, 20, 215–218.

Sacristán-Horcajada, S., Eugenia Arribas, M., Más, R. (2011): Sedimentología de sucesiones sinrift tempranas en un semigraben marginal de un rift extensional: la Cuenca de Bijuesca, Jurásico superior de la Cordillera Ibérica (Zaragoza, España). *Geogaceta*, 50-2: 121–124.

Sacristán-Horjacada, S., Carrasco, A., Mas, R., Arribas, M.E. (2012): Comparación del registro estratigráfico de dos cubetas satélites aso- ciadas a un sistema de *rift*: los surcos de Bijuesca y Bigornia (SE de la Cuenca de Cameros). *Geo-Temas* 13 (2): 155-158 (02_108-111 in CD).

Salas, R., Guimerà, J., Mas, R., Martín-Closas, C., Meléndez, A., Alonso, A. (2001): Evolution of the Mesozoic Central Iberian Rift System and its Cainozoic inversion (Iberian chain). In: P.A. Ziegler, W. Cavazza, A.H.F. Robertson, S. Crasquin-Soleau (eds.), *Peri-Tethys Memoir 6: Peri-Tethyan rift/wrench basins and passive margins.* Mémoires du Musée nat. Hist. naturelles de Paris 186, 145–185.

Salomon, J. (1982): Cameros-Castilla: El Cretácico Inferior. In A. García (Ed.), *El Cretácico de España* (pp.

345–387). Madrid: Univ. Complutense de Madrid.

San Román, J., Aurell, M. (1992): Palaeogeographical significance of the Triassic–Jurassic unconformity in the north Iberian basin (Sierra del Moncayo, Spain). *Palaeogeography, Palaeoclimatology, Palaeoecology*, 99, 101–117.

Schudack, M. (1987): Charophyten flora und fazielle Entwicklung der Grenzschichten mariner Jura-Wealden in den Nordwestlichen Iberi- schen Ketten (mit Vergleichen zu Asturien und Kantabrien). *Palaeontographica Abteilung B* 204, 1–180.

Schudack, U., Schudack, M. (2009): Ostracod biostratigraphy in the Lower Cretaceous of the Iberian chain (Eastern Spain). *Journal of Iberian Geology* 35, 141–168.

Soria, A.R., Martín-Closas, C., Meléndez, A., Meléndez, N., Aurell, M. (1995): Estratigrafía del Cretácico Inferior del sector central de la Cordillera Ibérica. *Estudios Geológicos* 51, 141–152.

Suárez-González P, Quijada IE, Benito MI, Mas R (2013): Eustatic versus tectonic control in an intraplate rift basin (Leza Fm, Cameros Basin): chronostratigraphic and paleogeographic implications for the Aptian of Iberia. *Journal of Iberian Geology* 39: 285–312.

Torcida Fernández-Baldor, F., Canudo, J.I., Huerta, P., Moreno-Azanza, M., Montero, D. (2017): *Europatitan eastwoodi*, a new sauropod from the Lower Cretaceous of Iberia in the initial radiation of somphospondylians in Laurasia. *PeerJ*, 5:e3409.

FIGURES

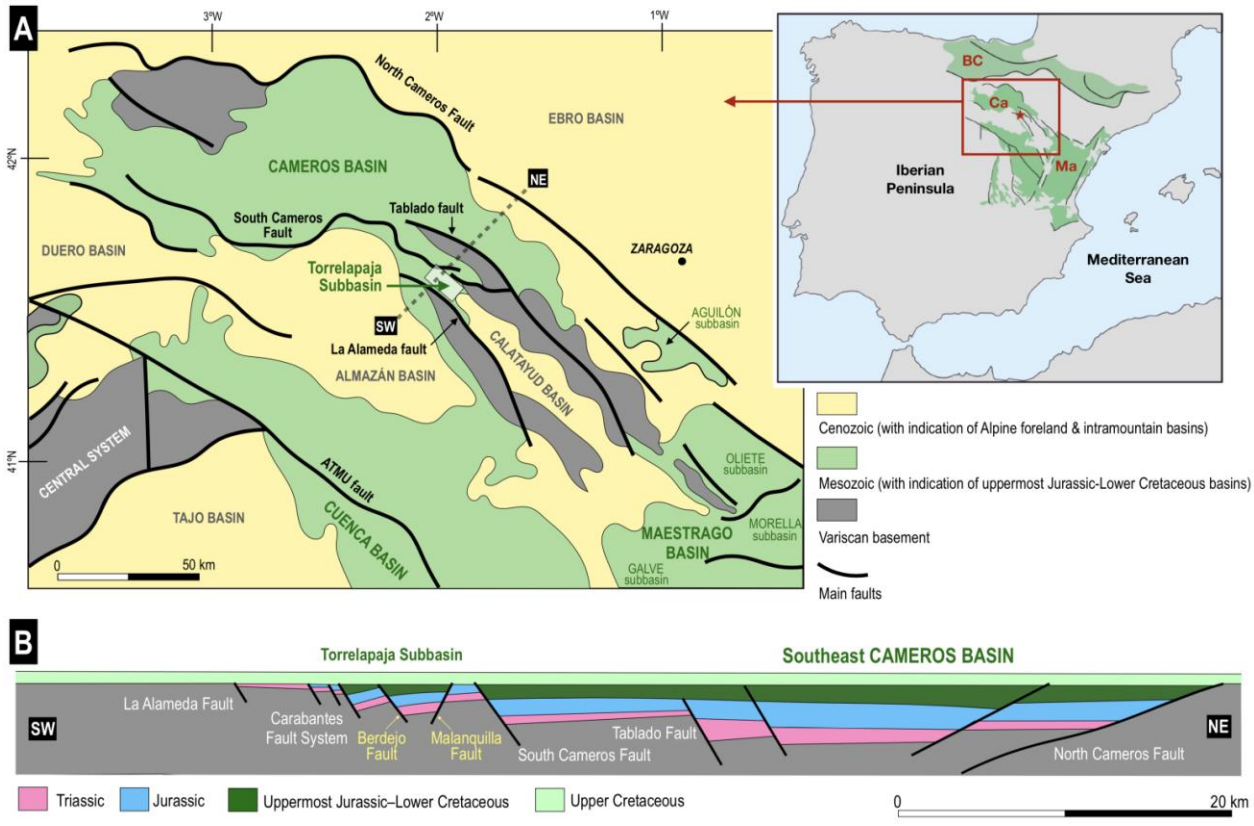

Fig. 1. - (A) Geological location of the Torrelapaja Subbasin. The map of the Iberian Peninsula shows the distribution of Mesozoic outcrops and the location of three main uppermost Jurassic-Lower Cretaceous sedimentary domains of Northeast Iberia: Maestrazgo (Ma), Cameros (Ca) and Basque-Cantabrian (BC) basins; (B) Geological restored section at the end of Mesozoic extension through the eastern part of the Cameros Basin (see dashed line in A for location). Modified from Guimerà et al. (2004), with reconstruction of the Torrelapaja Subbasin based on data exposed in this work.

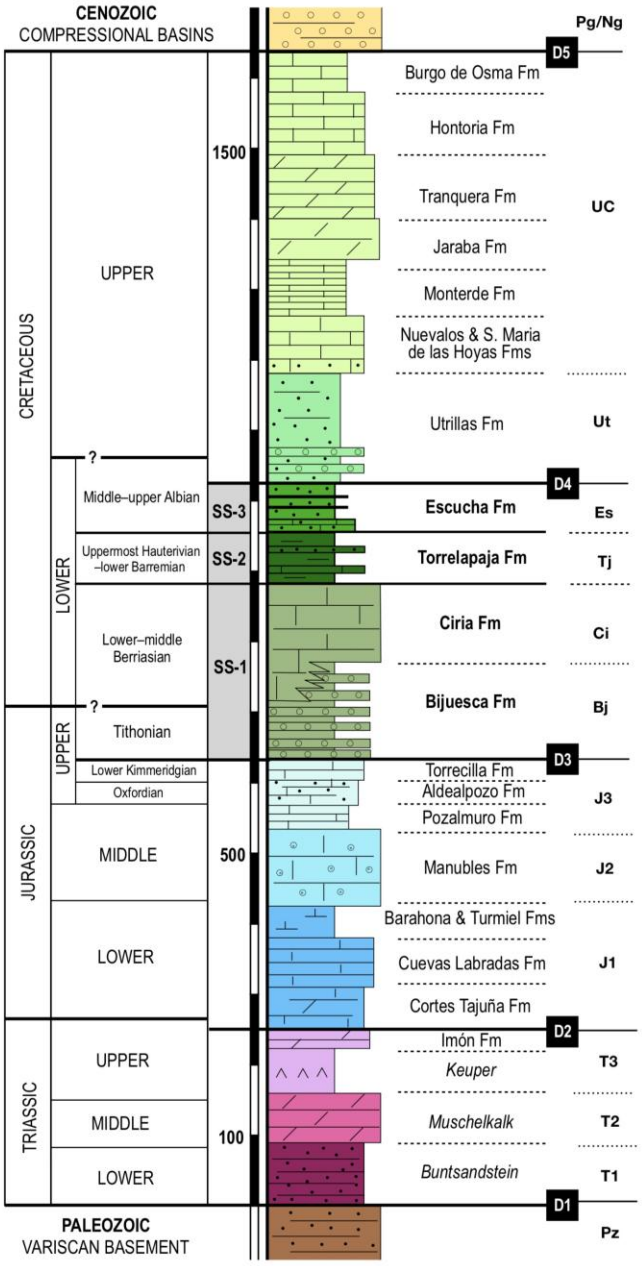

993

994 Fig. 2. - Summary of the stratigraphy of the Torrelapaja Subbasin. Major discontinuities D1–D5 separate
995 the successive synrift and postrift Mesozoic sequences. Abbreviated names of units of right column refer
996 to those used in the geological mapping of Figure 4. The studied synrift sequences (SS) shadowed in gray
997 in the central column are very variable in thickness.

998

999

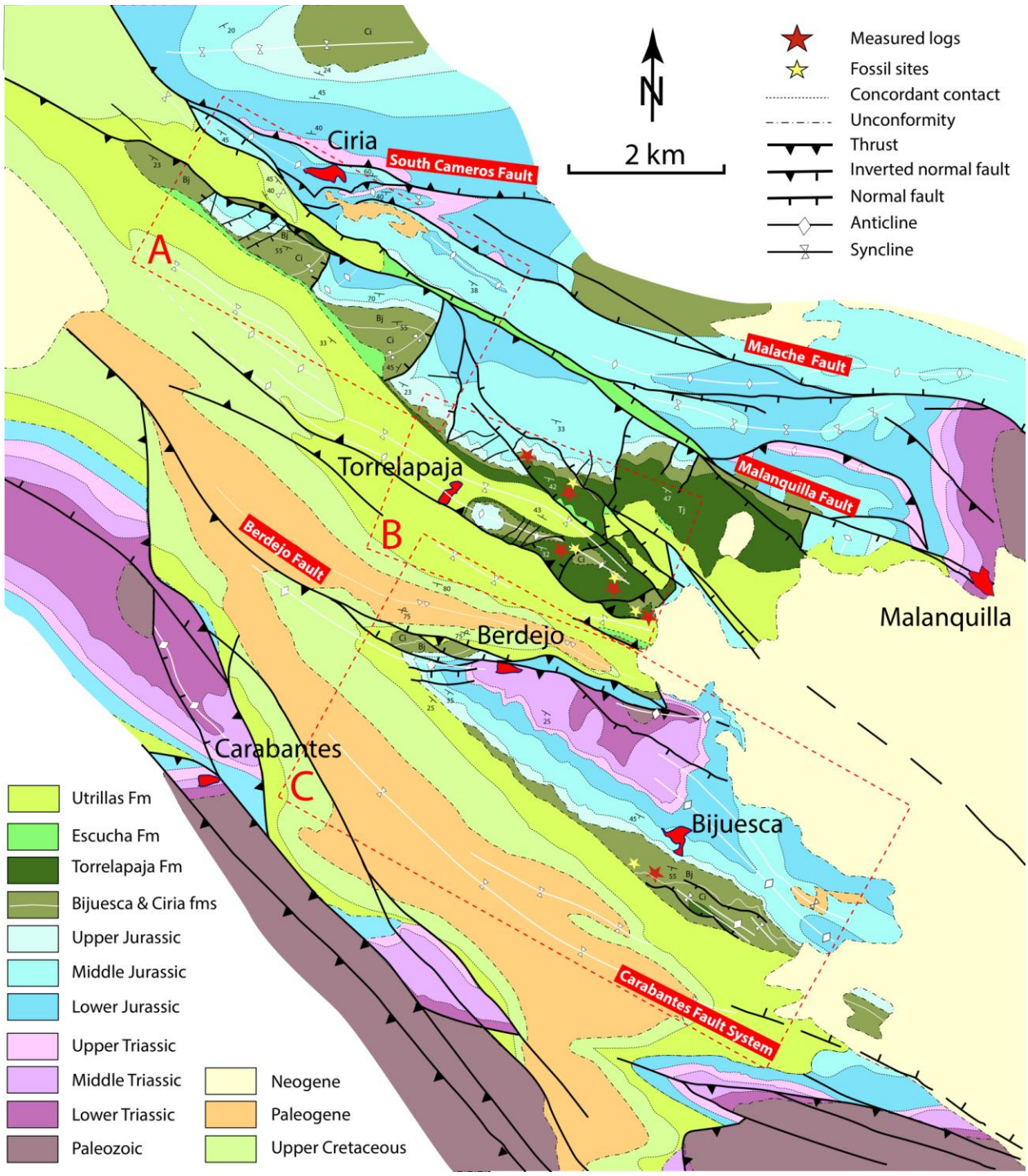

1000

1001 Fig. 3. - Geological mapping of the area including the Torrelapaja Subbasin. The mapping of the squared

1002 areas A, B and C is enlarged in Figure 4.

1003

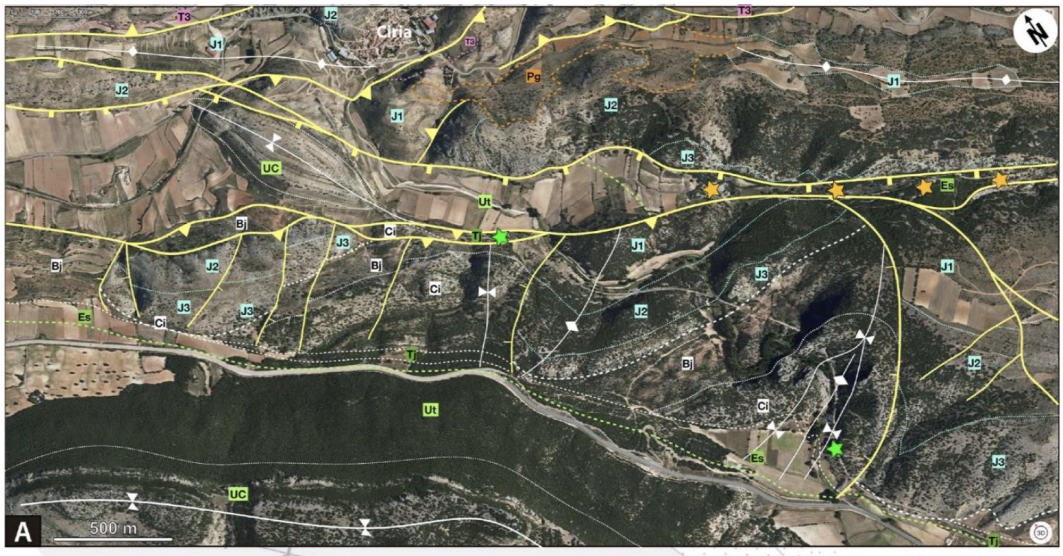
Ciria
T3
J2
J1
Pg
UC
Ut
Bj
Ci
Tj
Es
J3
500 m
A

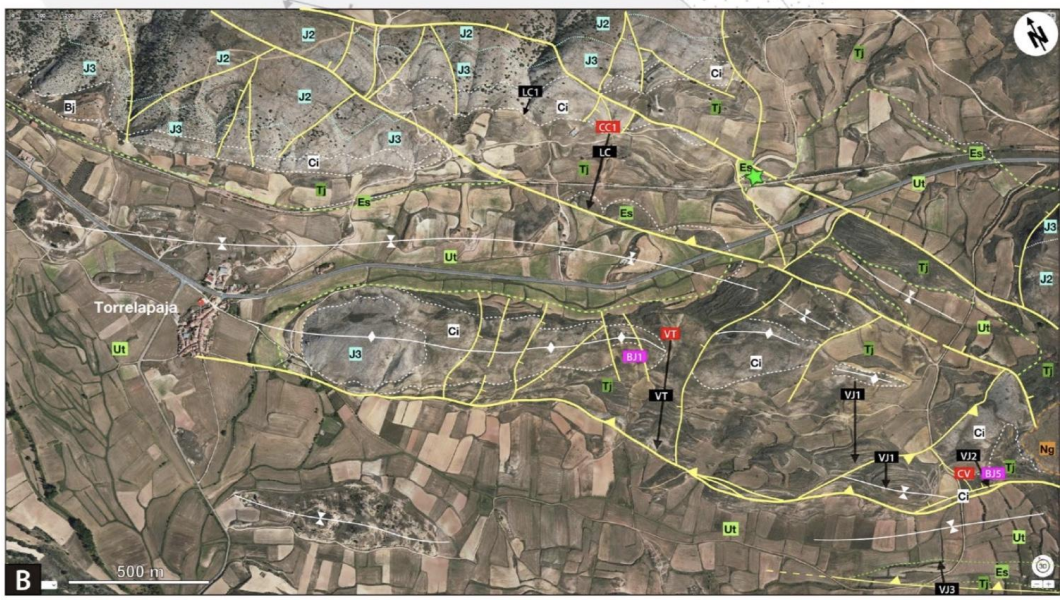
Torrelapaja
LC1
CC1
LC
VT
BJ1
VJ1
VJ2
CV
BJS
VJ3
Ng
500 m
B

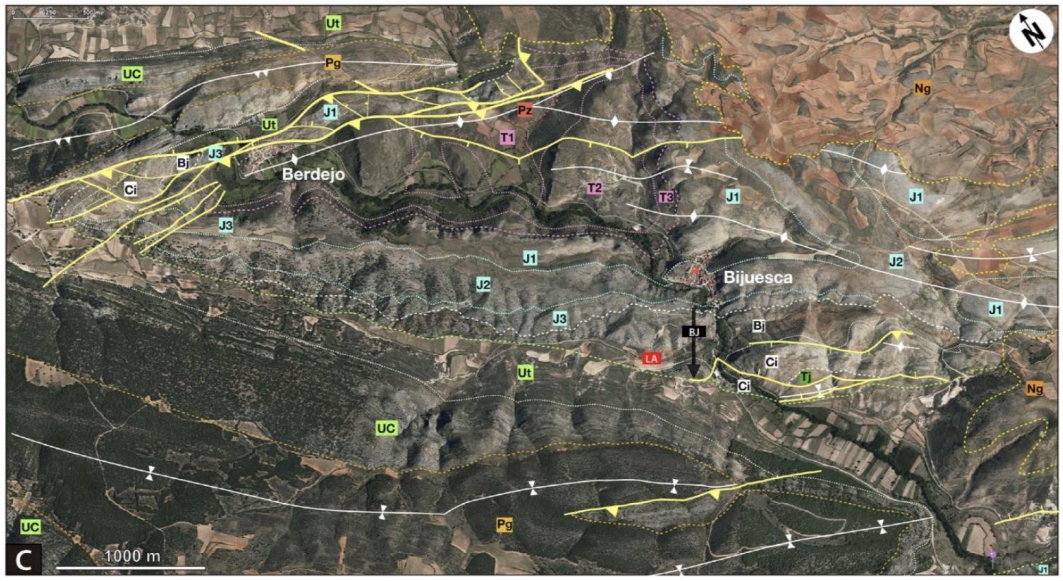
Berdejo
Bijuesca
Pz
T1
T2
T3
BJ
LA
Ng
UC
1000 m
C

Fig. 4. – Detailed geological mapping of some key areas (see Figs. 2 and 3 for legend of stratigraphic units and location). (A) Northern area: the orange stars locate in the abandoned coal mines in the upper Escucha Fm; the two green stars indicates the sampling points for charophytes of Martín-Closas (1989) in the Ciria and Torrelapaja formations respectively; (B) Central area: the black arrows indicate the location of La Cañada (LC), Valdelatorre (VT) and Valdelavieja (VJ) logs in the Torrelapaja Fm; the red squares indicate the new fossil sites of Corrales de Las Cañadas (CC), Valdelatorre (VT) and Corrales de Valdelavieja (CV); the pink squares correspond to the fossil sites BJ1 and BJ5 of Royo-Torres et al. (2012), the red squares indicate the new dinosaur fossil sites of Corrales de Las Cañadas (LC), Valdelatorre (VT), Valdelavieja (VJ) in the Torrelapaja Fm (see Fig. 10 for their stratigraphic location); the green star in B is the sampling point for the *Exogyra* shells used in the strontium analysis of the Escucha Fm; (C) Southern area with location of the Bijuesca (BJ) log and the new discovered fossil site of La Atalaya (LA) in the Bijuesca Fm (see red square).

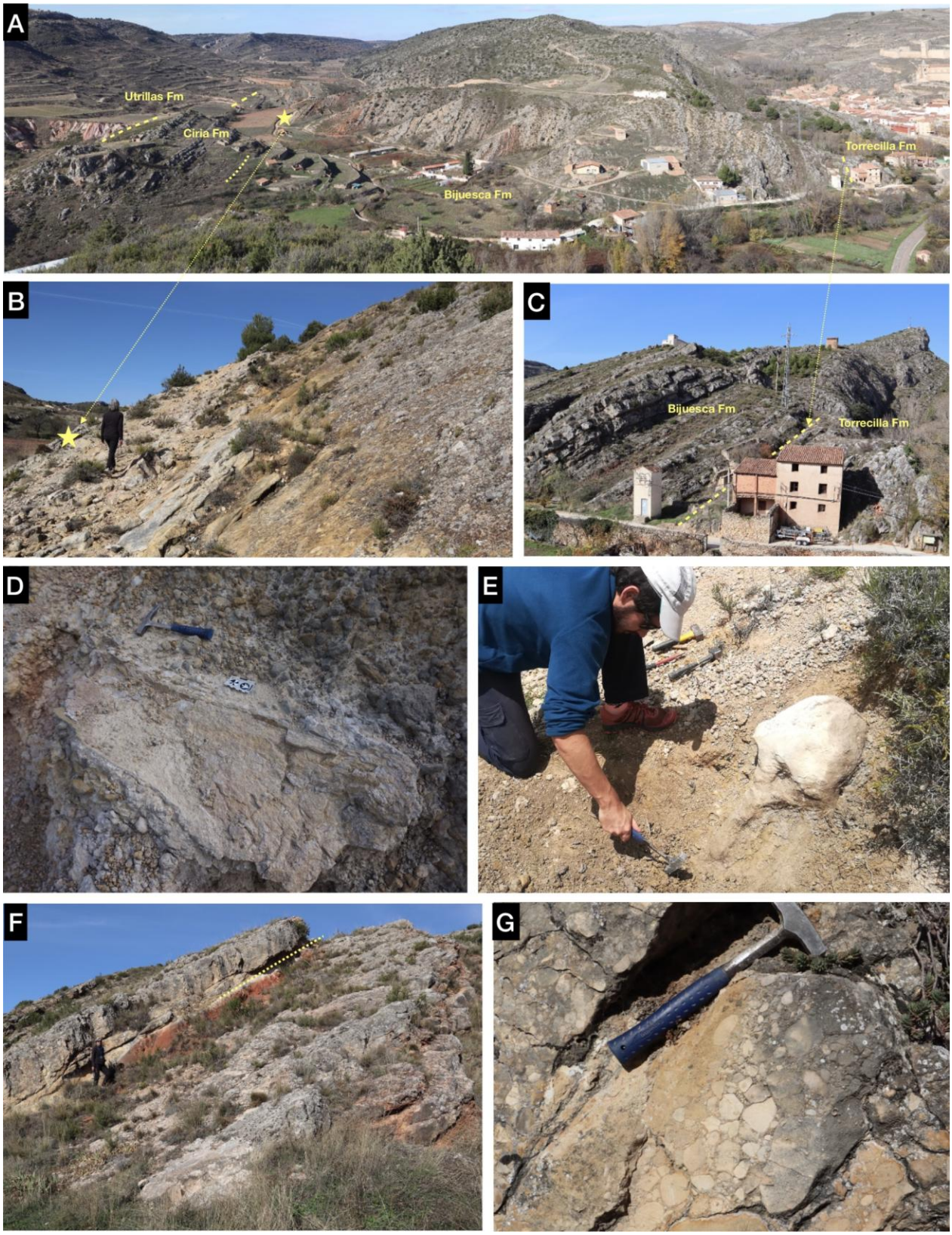
A
Utrillas Fm
Ciria Fm
Bijuesca Fm
Torrecilla Fm
B
C
Bijuesca Fm
Torrecilla Fm
D
E
F
G

1018

1019

Fig. 5. - The synrift sequence 1 in the Bijuesca trough. (A) General view of the Bijuesca outcrop, showing the distribution of units. The left part shows the angular unconformity with the Utrillas Fm. The yellow star locates the La Atalaya fossil site in the topmost levels of the Bijuesca Fm; (B) Fining-upward sequence in the upper Bijuesca Fm, ending with nodular/brecciated limestones with root traces. The yellow star indicates the carbonate level including La Atalaya fossil site (see Fig. 10 for its stratigraphic location); (C) Detail of the paraconformity between the lower Kimmeridgian reef limestones of the Torrecilla Fm and the conglomerates, sandstones and mudstones of the Bijuesca Fm; (D) Large-sized limb bone fragment assigned to Sauropoda indet floating in a nodular/brecciated limestones in La Atalaya site; (E) Large-sized caudal vertebra assigned to Sauropoda indet. encased in burrowed marls in La Atalaya site; (F) A fining-upward sequence from conglomerates to sandstones to red mudstones in the upper Bijuesca Fm; (G) Close view of clast-supported conglomerates with poorly rounded Jurassic limestone clasts with normal gradation in the middle part of the Bijuesca Fm.

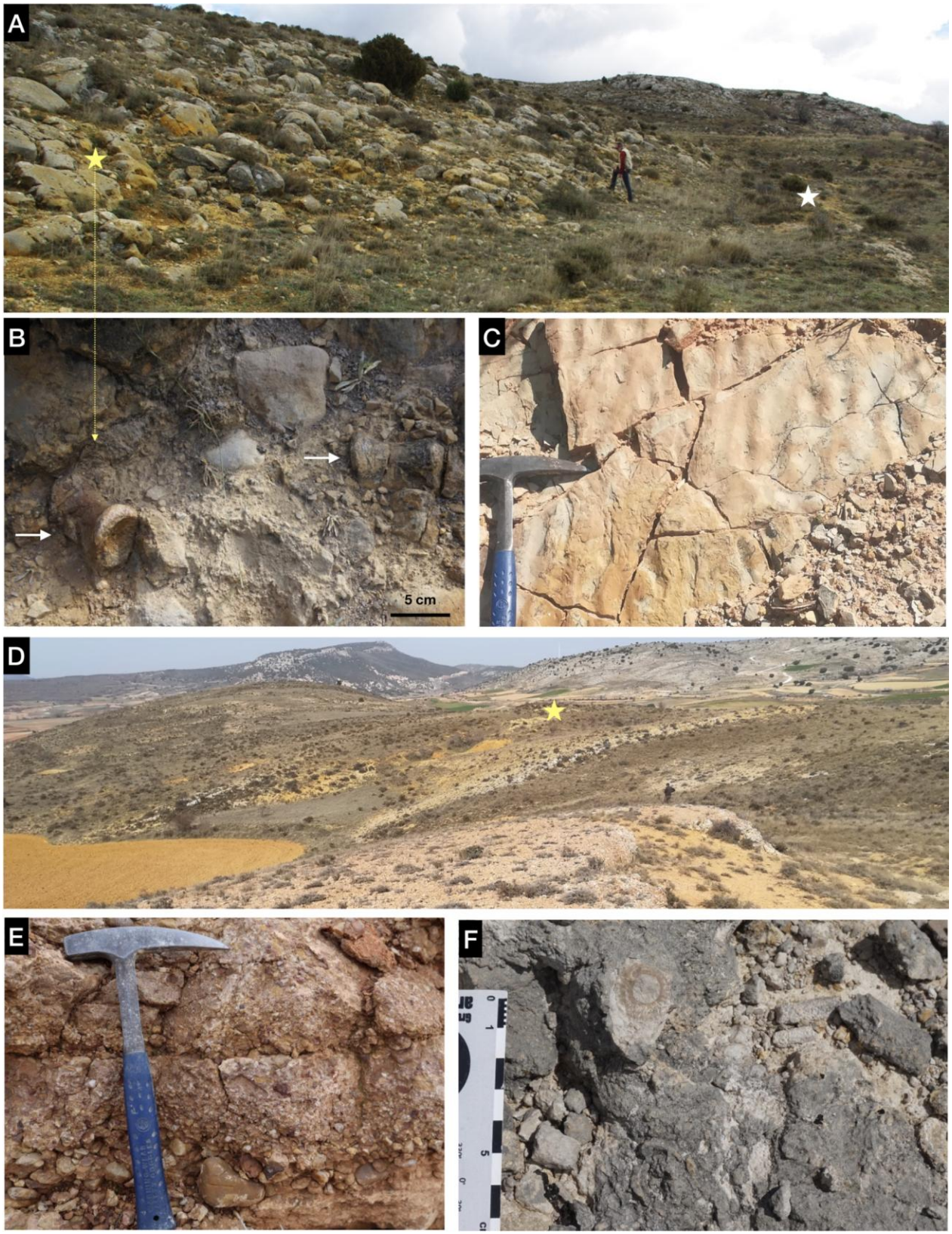

1032

1033

Fig. 6. - The synrift sequence 2 in the outcrops located around Valdelavieja-Valdelatorre logs. (A) Highly irregular paleokarst developed on top of the Ciria Fm in Valdelavieja log, including the fossil site of CV. The overlying level (white star) includes the samples CV-2 and CV-3 (see fig. 10); (B) The infill of the karst cavities in Valdelavieja has yield two theropod? vertebrae (see white arrows) and other remains; (C) Rippled sandstones in the middle part of the Torrelapaja Fm; (D) General view of the outcrop of Valdelatorre exposing the ochre marlstones/calcareous mudstones of the lower part of the Torrelapaja Fm. The yellow star indicates the location of the Berdejo-1 (BJ-1) fossil site of Royo-Torres et al. (2012); (E) Close view of the grain-supported conglomerates with quartzite clasts and normal gradation found in the middle part of the Torrelapaja Fm in the Valdelavieja log; (F) Close view of the tufa level with abundant debris of coated plant stems exposed in the upper part of the Torrelapaja Fm in the Valdelatorre log.

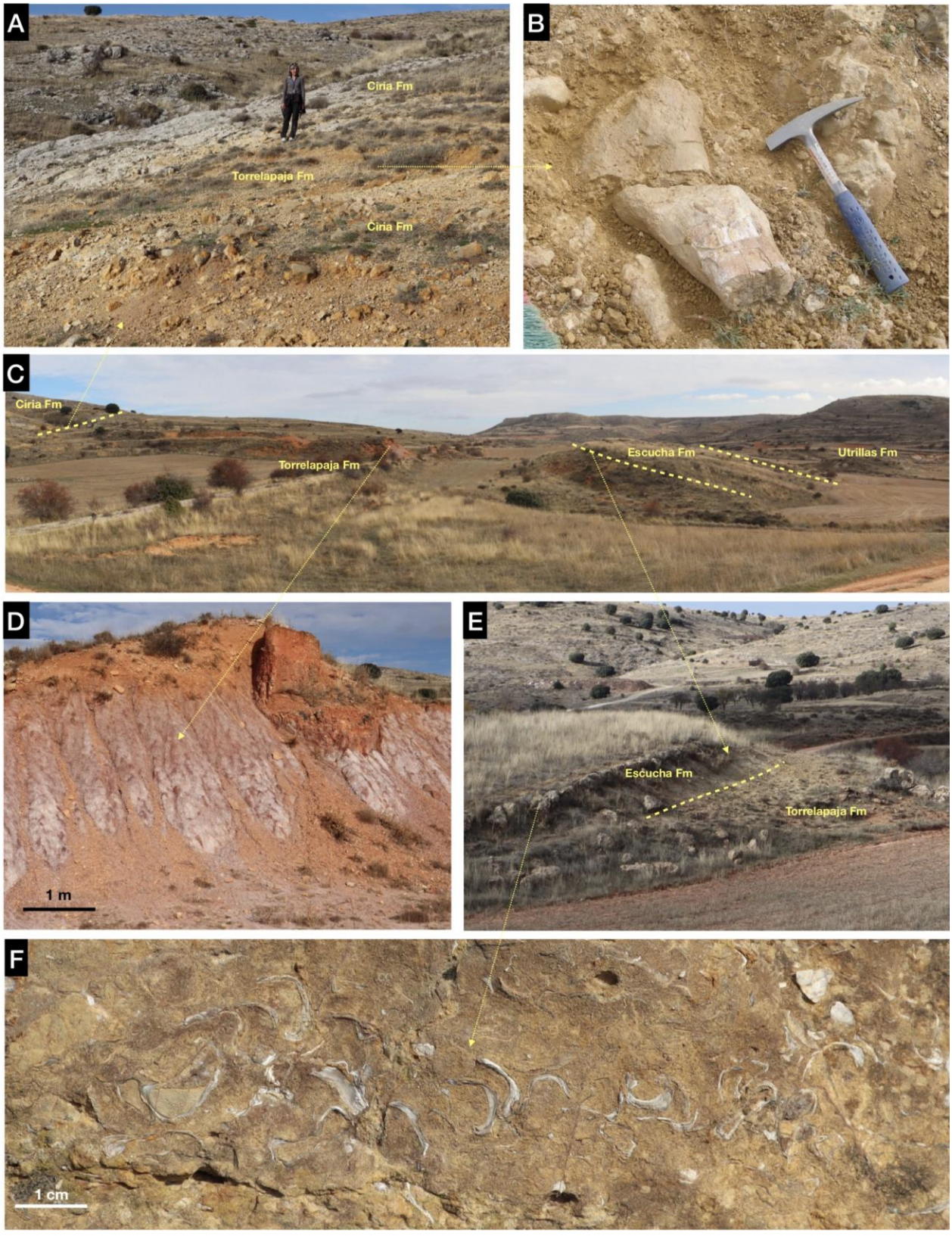
A
Ciria Fm
Torrelapaja Fm
Ciria Fm
B
C
Ciria Fm
Torrelapaja Fm
Escucha Fm
Utrillas Fm
D
1 m
E
Escucha Fm
Torrelapaja Fm
F
1 cm

1047

1048

1049 Fig. 7. - Field views of Las Cañadas log. (A) Large karst cavity developed on top of the Ciria Fm filled by
1050 reddish mudstones; (B) Close view of the sauropod humerus recovered in the paleokarstic cavity of Las
1051 Cañadas; (C) General view of the outcrop of Las Cañadas; (D) Red mudstones with hydromorphic soils of
1052 the upper part of the Torrelapaja Fm in Las Cañadas log; (E) Boundary between SS-2 (Torrelapaja Fm) and
1053 SS-3 (Escucha Fm) in Las Cañadas outcrop; (F) Sandy skeletal limestone rich in oyster shells typical of the
1054 lower part of the Escucha Fm.

1055

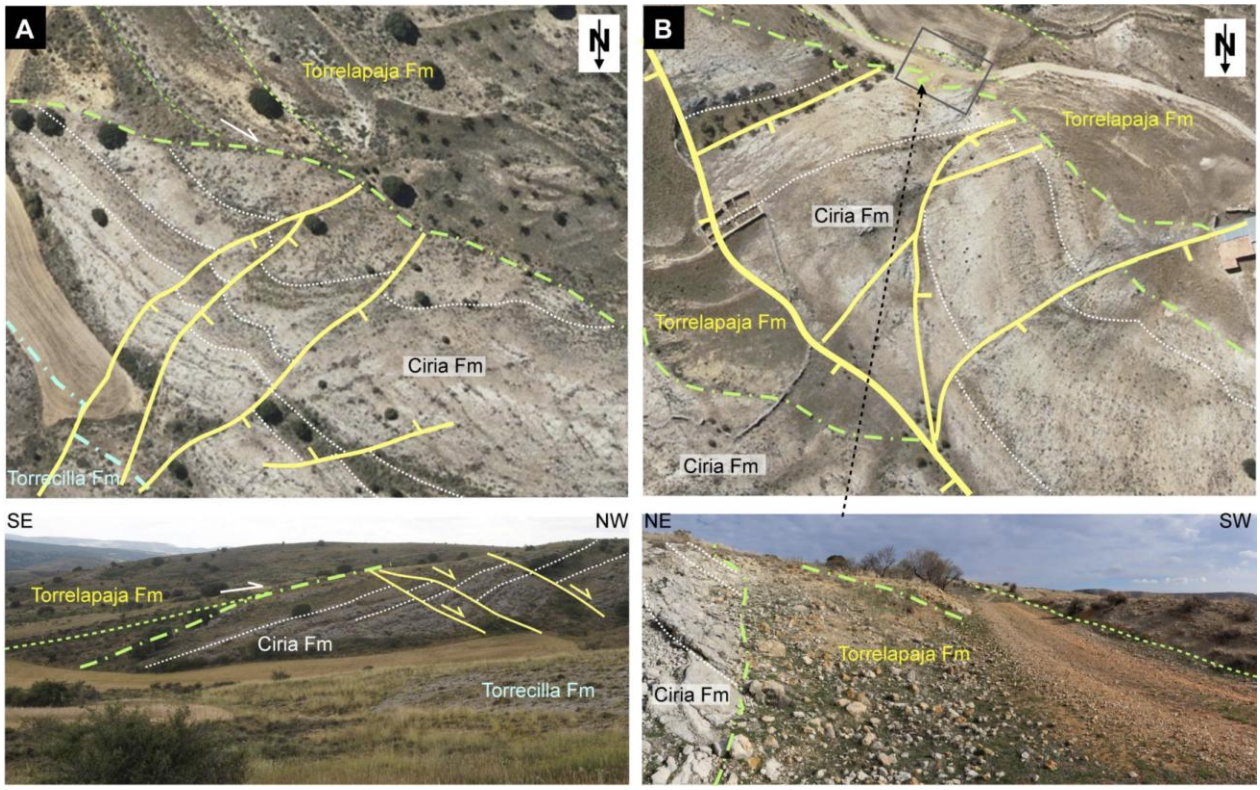

1056

1057 Fig. 8. – Oblique aerial view (above) and outcrop image (below) of two examples showing the angular
1058 unconformity between SS-1 (Ciria Fm) and SS-2 (Torrelapaja Fm) in the southeastern part of the Bigornia
1059 trough. The example of the right includes the Corrales de Las Cañadas fossil site. Note as the angular
1060 unconformity fossilizes decametric-scale normal faults affecting the Ciria Fm limestones, and the lower
1061 Torrelapaja Fm beds onlap the unconformity.

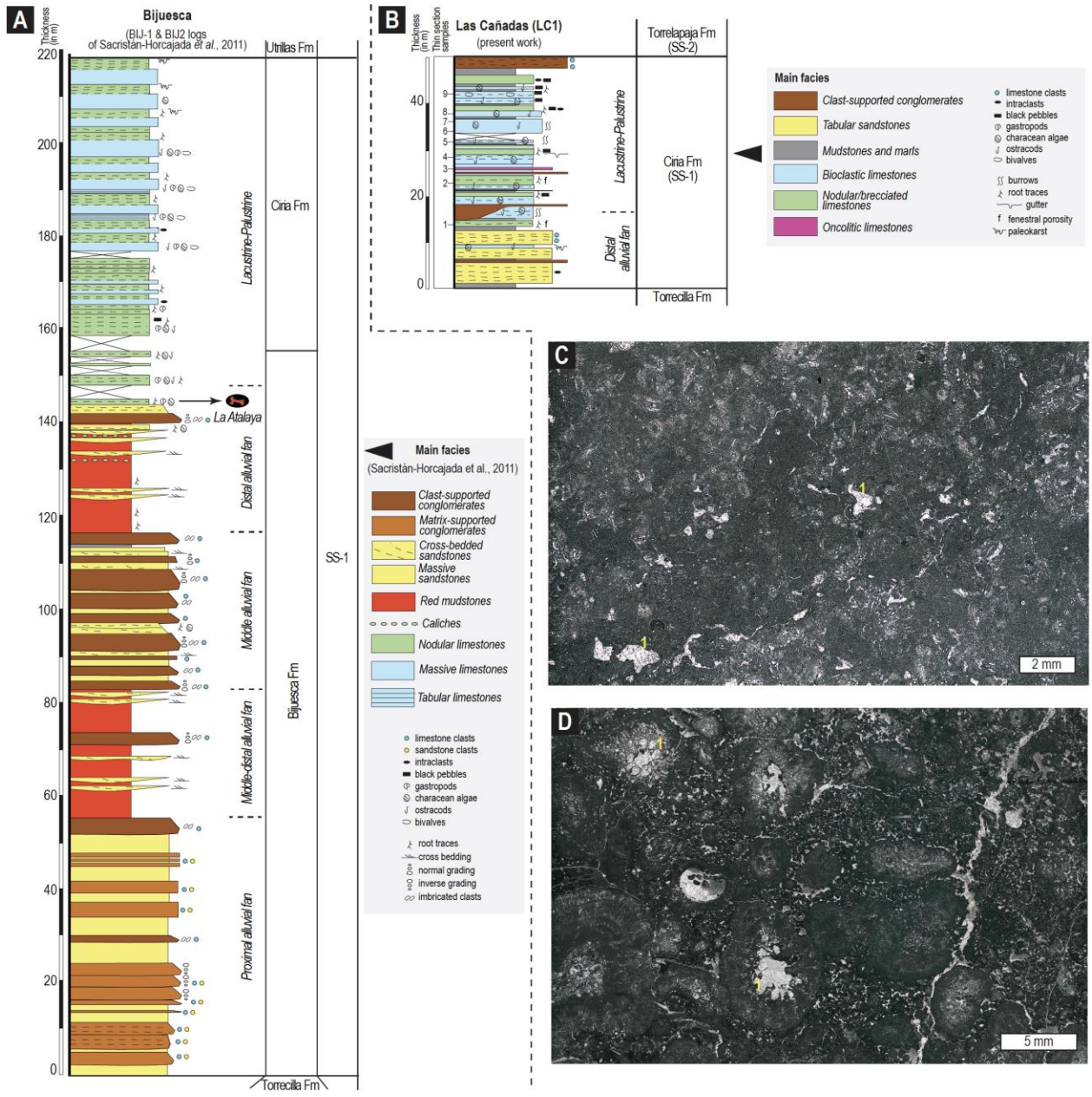

Fig. 9. - Sedimentological features of the Bijuesca and Ciria formations. (A) Stratigraphic log indicating the facies distribution of the Bijuesca and Ciria formations in Bijuesca locality (redrawn and slightly modified from Sacristan-Horcajada et al., 2011; see BJ in Fig. 4C for location), and the location of La Atalaya fossil site; (B) Stratigraphic log indicating the facies distribution of the Ciria Fm in Las Cañadas 1 log (LC1; see Fig. 4B for location); (C-D) Thin section images in plane-polarized light of limestone facies of the Ciria Fm: (C) palustrine limestones with charophytes and fenestral porosity (see 1); and (D) oncolitic limestones with cm-thick oncoids with charophytes in the nuclei (see 1).

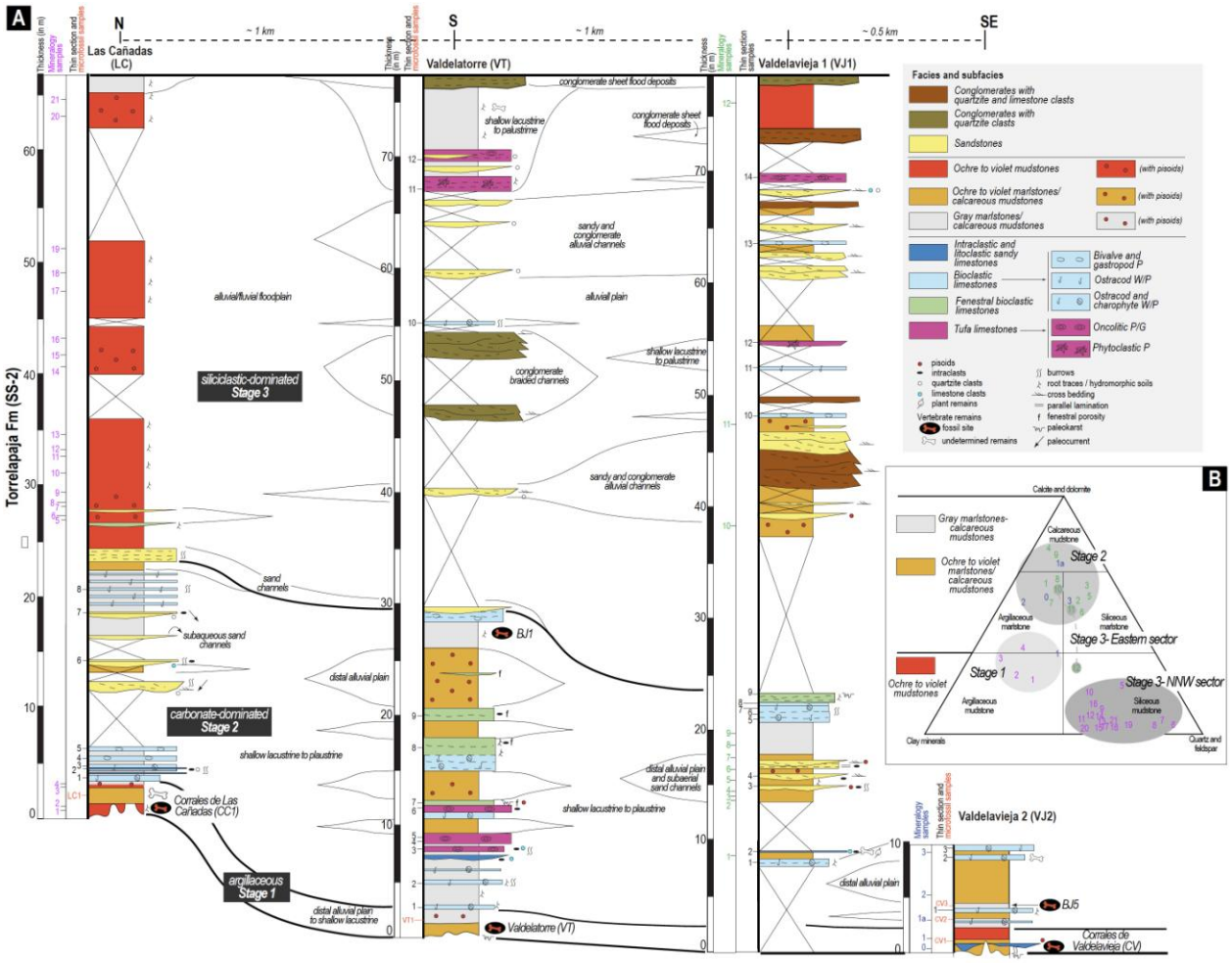

1070

1071 Fig. 10. - Sedimentological features of the Torrelapaja Fm. (A) Stratigraphic logs indicating the facies
1072 distribution of the Torrelapaja Fm (see Fig. 4B for location). The three sedimentary stages differentiated
1073 and the location of the fossil sites of Corrales de Valdelavieja (CJ), Valdelatorre (VT), Corrales de Las
1074 Cañadas (CC) and Berdejo-1 (BJ-1) are also indicated; (B) Mineralogical composition of muddy facies of
1075 the unit (tertiary diagram adapted from Allix et al., 2011).

1076

1077

1078

1079

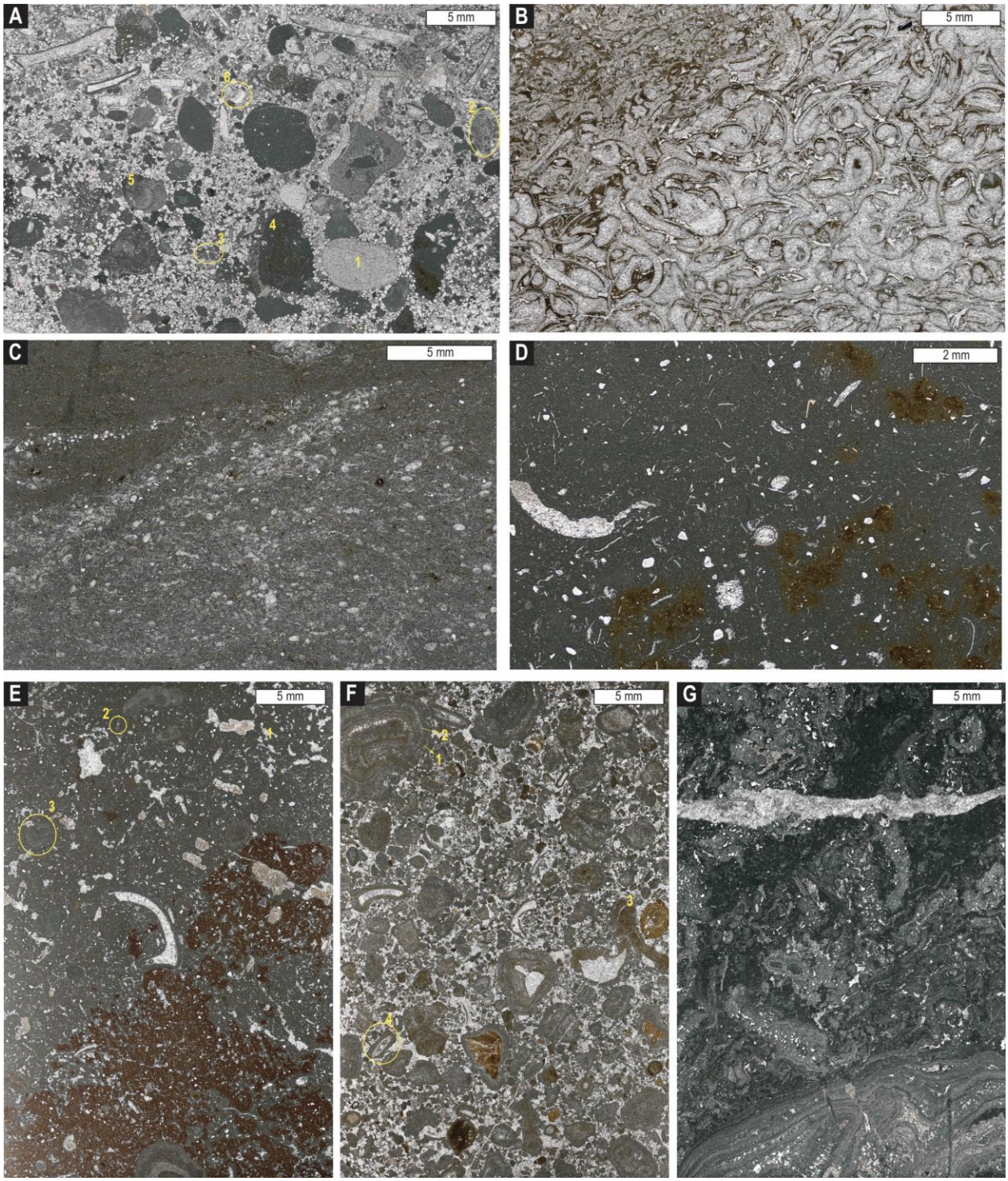

1080

1081 Fig. 11. Thin sections images in plane-polarized light of limestone facies of the Torrelapaja Fm. (A)

1082 Intraclastic/litoclastic facies with quartz sand and quartzite lithoclasts (Paleozoic: see 1), limestone

1083 (Jurassic) lithoclasts (see echinoid spine in 2 and ooids in 3), intraclasts of bioclastic facies (see 4), oncoid

1084 fragments (see 5) and vertebrate remains (see 6); (B–D) Lacustrine bioclastic limestones, including (B)

bivalve and gastropod packstone and (C) bioturbated ostracod wackestone/packstone, with accumulation of skeletal debris produced by hydrodynamic sorting; and (D) ostracod and charophyte wackestone; (E) Fenestral bioclastic limestone with ostracods and charophytes formed in palustrine areas. Notice fenestral porosity (see 1), charophytes (see 2) and oncoid fragments (see 3); (F-G) Tufa limestones including (F) oncolitic packstones/grainstones with entire and broken oncoids, with bioclastic and intraclastic cores and cortices formed by sub-mm to mm alternation dark micritic laminae (see 1), and porous micritic laminae with microbial filaments perpendicular to laminae (see 2), intraclasts of stromatolites (see 3) and coated plant stems (see 4); and (G) phytoclastic packstones big clasts of coated plant stems and stromatolites, in an packstone matrix of smaller intraclasts and oncoid fragments.

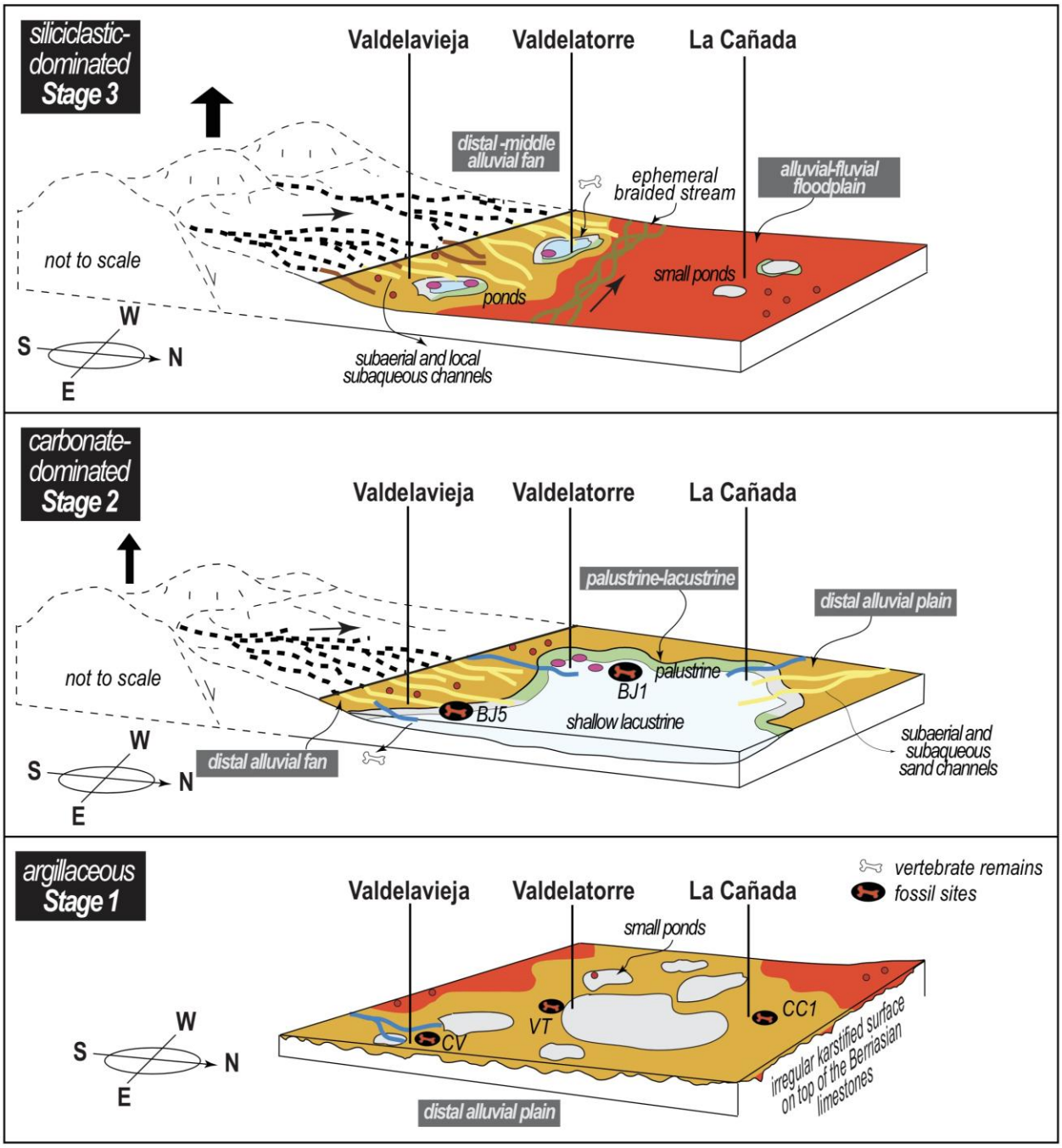

1095

1096 Fig. 12. Palaeoenvironmental reconstruction of facies of sedimentary stages 1 to 3 of the Torrelapaja Fm

1097 (see Fig. 10 for legend of facies).

1098

1099

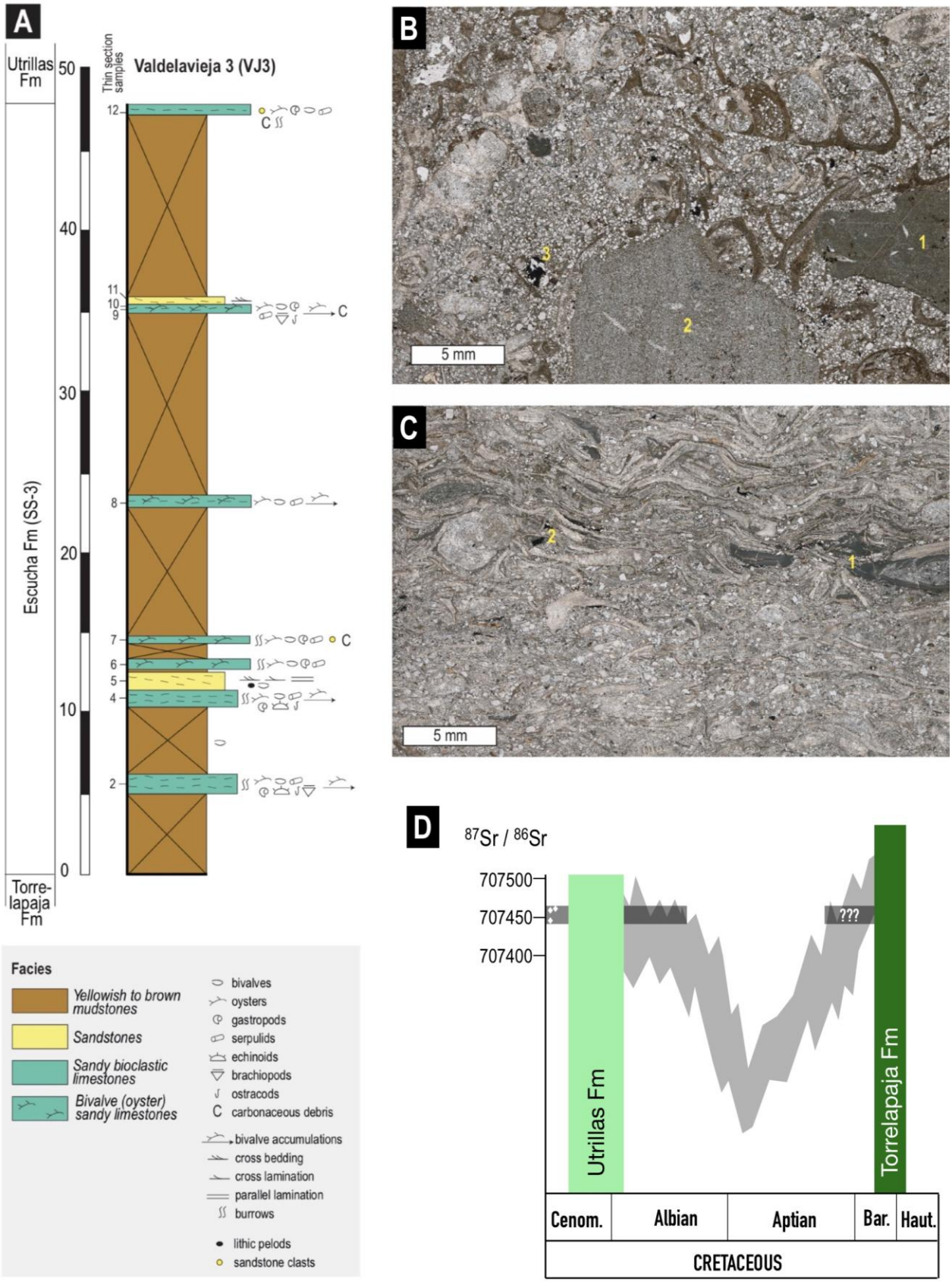

Fig. 13. (A) Sedimentological features of the Escucha Fm (SS-3) in the Valdelavieja 3 log (see VJ3 in Fig. 4B

for location); (B-C) Thin sections images in plane-polarized light of limestone facies, including (B) sandy blioclastic limestones, with abundant oysters and gastropods, intraclasts of muddy limestones (see 1) and sandstones (see 2) and carbonaceous material (see 3); and (C) bivalve sandy limestones, with accumulated debris of oysters, and some serpulids (see 1) and carbonaceous material (see 2). (D) Strontium isotopic curve of McArthur et al. (2012) during Barremian–Albian (in light gray) indicating the interval comprising the three values obtained from the Escucha Fm (withe diamonds, left part). Considering the time constrains provided by the Torrelapaja and Utrillas formations, the obtained isotopic values are compatible with two time intervals (see dark grey surface). However, regional data and overall palaeogeography of northeast Iberian clearly point to a middle-late Albian age for the Escucha Fm (see further explanation and discussion in text).

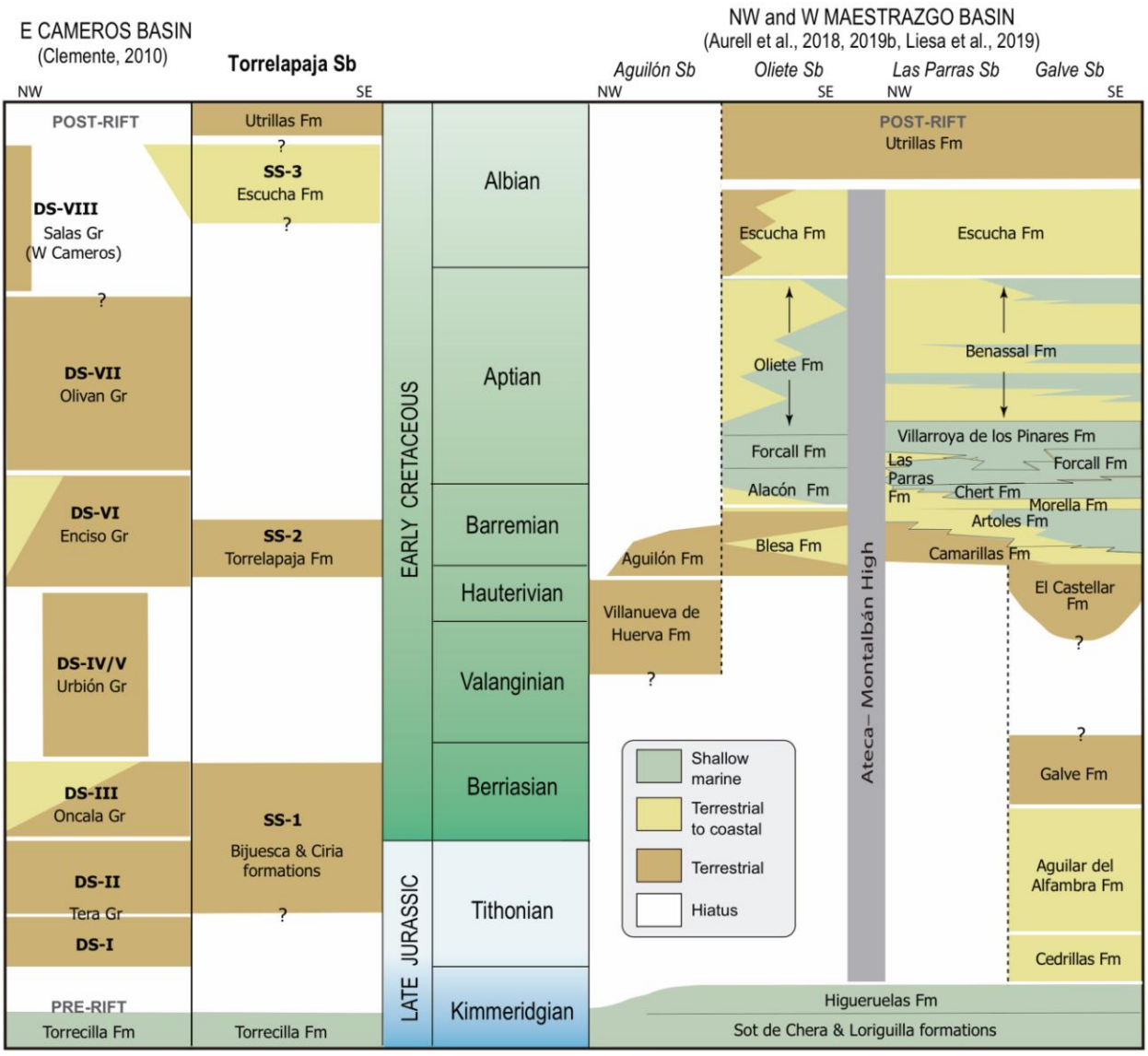

Fig. 14. Proposed equivalence between the synrift sequences recorded in the Torrelapaja Subbasin and those recorded in the eastern Cameros Basin (mostly based in Clemente, 2010) and the subbasins of the Western Maestrazgo Basin (compiled from Aurell et al, 2018, 2019b and Liesa et al., 2019; see fig. 1 for location of basins and subbasins).

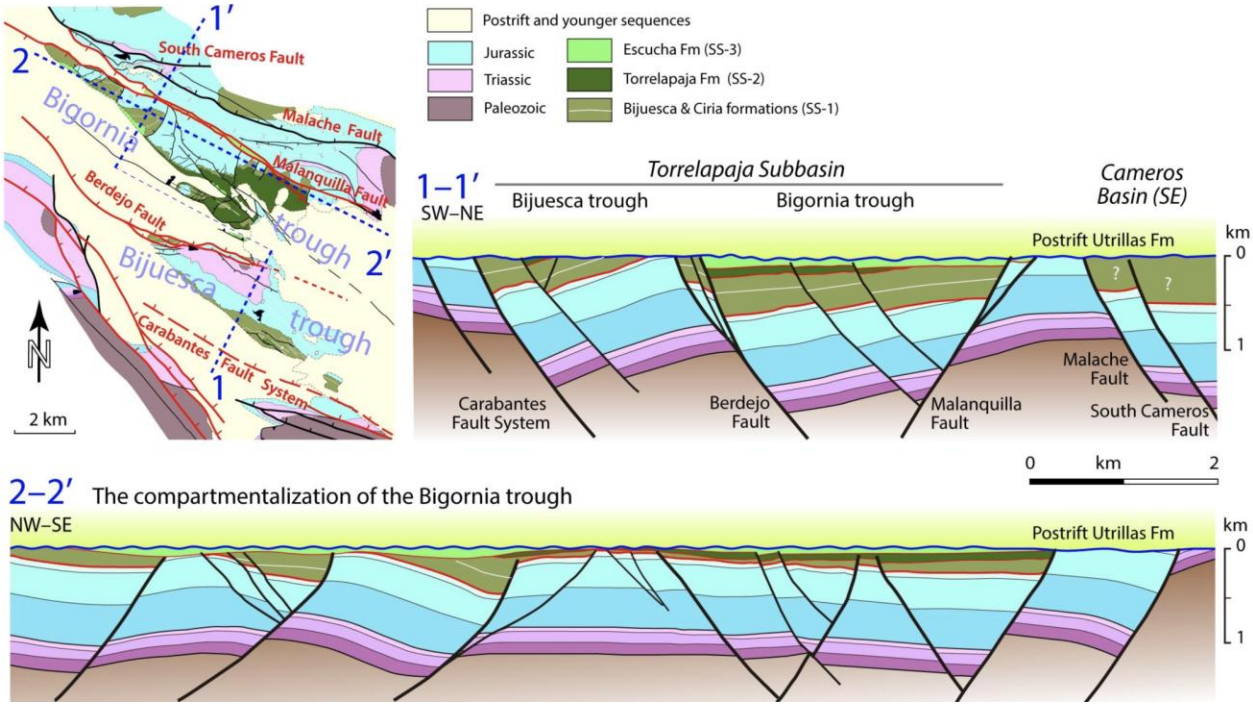

1121

1122 Fig. 15. Idealized geological cross-sections showing the structure of the Torrelapaja Subbasin at the time

1123 of postrift sedimentation (see map for location). 1-1': Transverse view of the Torrelapaja Subbasin

1124 showing the structure of the Bigornia and Bijuesca troughs. 2-2': Longitudinal section along the Bigornia

1125 trough. Note that the NE-SW Cenozoic shortening has not been restored.

1126

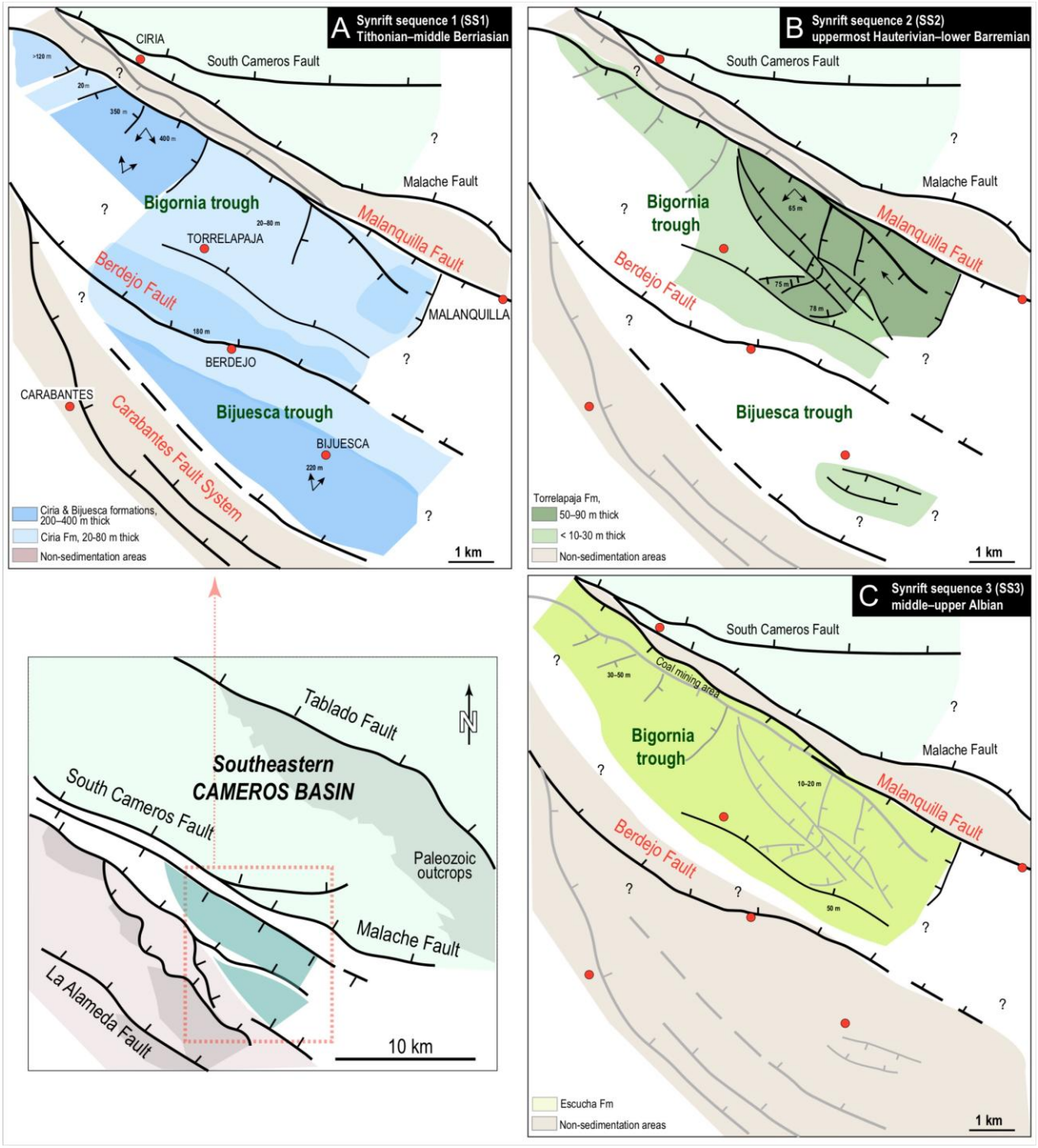

Fig. 16. - Reconstruction of the Bijuesca and Bigornia troughs (Torrelapaja Subbasin) located south of the South Cameros Fault (inset) during the sedimentation of synrift sequences (SS) 1, 2 and 3 (maps A, B and C respectively). Specific data of thickness measured in different localities are indicated. Arrows in A and B indicates palaeocurrent data (the data in SS-1 taken form Sacristán-Horcajada et al., 2012). Note that maps represent the present-day locations of structures and outcrops, that is without the restoration of

1133 the NE-SW Cenozoic shortening.

1134

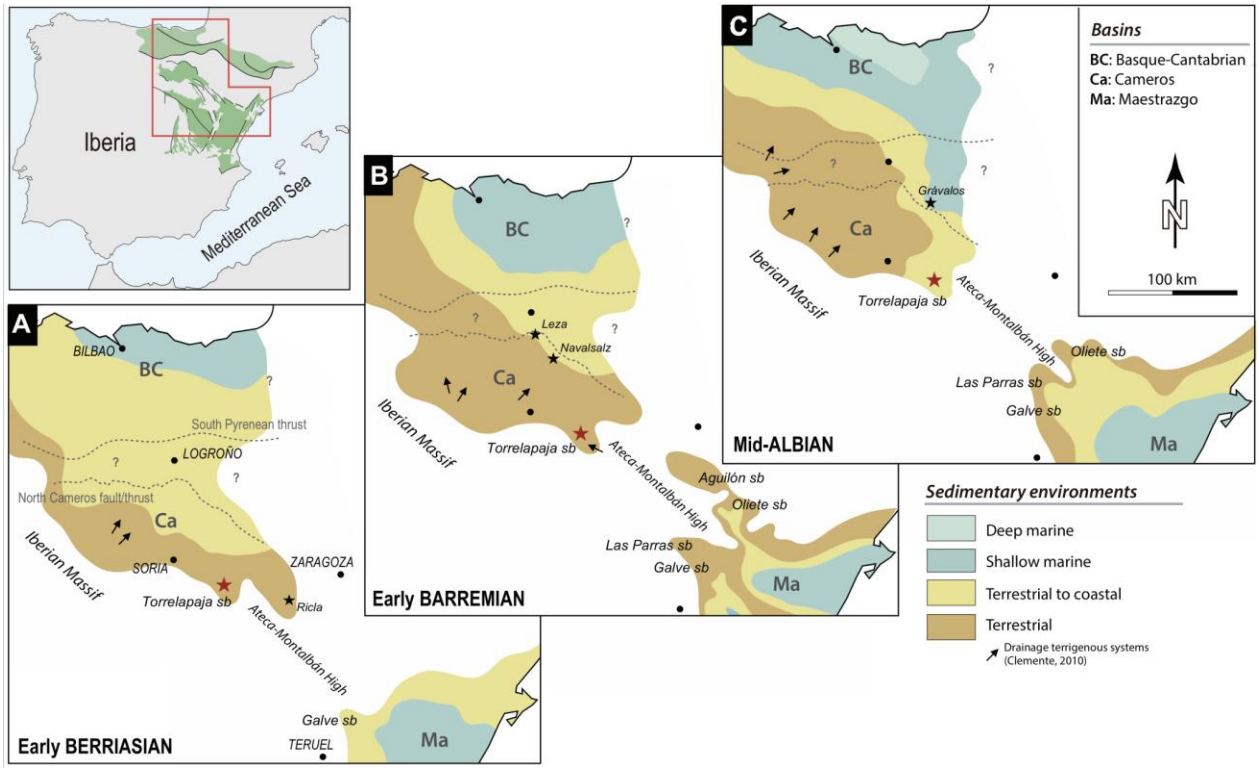

1135

1136 Fig. 17. Distribution of main sedimentary domains of Northeast Iberia around (A) the early Berriasian, (B)

1137 the early Barremian and (C) the mid-Albian. Palaeogeography of the Basque-Cantabrian Basin taken from

1138 García (1982), García-Mondejar (1990) and Pujalte et al. (2004). Cameros Basin compiled from Muñoz et

1139 al. (1997), Clemente (2010), Quijada et al. (2013) and Suárez-Gonzalez et al. (2013). Maestrazgo Basin

1140 based on Querol et al. (1992), Aurell et al. (2018, 2019b) and Liesa et al. (2019).